Varshney et al. Journal of Theoretical and Applied Physics 2012, 6:25
http://www.jtaphys.com/content/6/1/25

Journal of Theoretical and Applied Physics
a SpringerOpen Journal

REVIEW Open Access

Phonon-induced superconductivity and physical properties in intercalated fullerides Rb_3C_{60}

Dinesh Varshney[1*], Rajendra Jain[1] and Namita Singh[2]

Abstract

The nature of electron pairing mechanism and physical properties leading to superconducting state and normal state resistivity in alkali metal (Rb) intercalated fullerenes are explored. Keeping in mind that free electrons in lowest molecular orbital are coupled with inter-molecular phonons, the coupling with inter-molecular phonon leads to transition temperature (T_c) of about 4.17 K. The electrons also couple with the intra-molecular phonons. Within the framework of strong coupling theory, T_c is estimated at 34 K. The carbon isotope effect exponent, the energy gap ratio, influence of pressure and volume on T_c, and thermodynamical parameters describing the superconducting state confer that Rb_3C_{60} as *s*-wave superconductor. Estimated contribution to resistivity using scattering with inter- and intra-molecular phonon, when subtracted from single crystal data, infers quadratic temperature dependence over most of the temperature range and is attributed to electron–electron inelastic scattering. Both low frequency intermolecular and high frequency intra-molecular phonons have significant bearing in Rb_3C_{60} superconductor.

Keywords: Fullerenes, Inter- and intra-molecular phonons, Transition temperature, Carbon isotope effect, Energy gap ratio

Review

Introduction

Superconductivity in alkali metal intercalated Buckminster fullerenes with superconducting transition temperature (T_c is approximately 20 to 45 K) continues to provoke considerable interest [1-3]. The nature of attractive pairing mechanism with conventional phonon-mediated electron pairing or unconventional electronic mechanisms in superconducting fullerides is, of course, a central point of several experimental studies, which remains unsettled for a quite long time. The normal state electronic and magnetic properties of alkali metal intercalated fullerides (AMIF) are still only partially understood and are reviewed at great length [4,5]. Despite massive experimental and theoretical efforts, consistent picture of pairing mechanism leading to a superconducting as well as anomalous physical properties needs more attention. Apart from the understanding of the unusual properties, the doping in C_{60} as M_xC_{60} (M = K, Rb, Cs, and x = 1,2, and 3) is at the center of many novel phenomena and hence points to their technological and industrial importance.

Neutron inelastic scattering measurements [6,7] and Raman spectroscopy [8] have been extensively used to probe the molecular vibrational modes of C_{60} in pristine and doped C_{60} solids, in investigation of structural and electron–phonon interaction, and in superconducting fullerides. The AMIF have a wide frequency range of phonon spectrum. Neutron scattering indicated that the vibrational spectrum of Rb_3C_{60} may be divided into two regions. One of them belongs to the rotation of C_{60} molecule, the inter-molecular vibrations being in the range of 2 to 20 meV and another is the intra-molecular mode with frequency from 25 to 200 meV. Raman scattering yields the on-ball vibrational modes (approximately 40 meV to 0.2 eV). The phonon spectrum in AMIF consists of mode of C_{60} (26 cm^{-1}), the vibrations of Rb^+ ions and the translational vibrations as a whole (approximately 15 to 150 cm^{-1}), and the on-ball molecule vibrations (approximately 400 to 1,400 cm^{-1}) as revealed from lattice dynamic studies [9]. The electron–phonon interaction is usually assumed to cause the superconductivity. It should, however, be important to clarify

* Correspondence: vdinesh33@rediffmail.com
[1]Materials Science Laboratory, School of Physics, Vigyan Bhawan, Devi Ahilya University, Khandwa Road Campus, Indore 452001, India
Full list of author information is available at the end of the article

which of these molecular vibrational modes plays a major role in yielding a superconducting state.

The energy scales of the various phonon modes that mediate the electron–phonon coupling are different, owing the dependence of superconducting transition temperature on isotopic mass, a good probe to clarify phonon mechanism. Precise measurement of carbon isotope allows us to know whether on-ball molecular phonons, alkali-C_{60} optic phonons, and translational modes of AMIF play a major role on the electron–phonon coupling or not. The carbon isotope effect demonstrates $\alpha_c = 0.37 \pm 0.05$, with the 75% ± 5% substitution of $^6C_{13}$ for $^6C_{12}$ [10] naturally favors the phonon-mediated pairing, which rules out the electronic one. Fuhrer and coworkers reported a reduced α_c of about 0.21 ± 0.012 [11]. It is apparent that conventional BCS weak coupling theory predicts one half value of isotope effect, and reduced value indicates that the BCS model must be modified. It is fair to note that although carbon isotope effect demonstrates the role of phonons, it does not tell whether these modes are intra-molecular or inter-molecular.

We note that the Rb dopant isotope effect measurements verify that inter-molecular phonons do not play a significant role in AMIF [10]. Along with the carbon isotope effect exponent, it clearly demonstrates the unique role of intra-molecular phonons as far as the origin of superconductivity in fullerides is concerned. Burk and coworkers have shown a Rb isotope effect of $\alpha_{Rb} = -0.028 \pm 0.036$, a result which implies that the alkali-C_{60} optic phonons play, at most, a minor role in the pairing mechanism [12]. However, a substantial intercalant isotope effect is expected in a situation with significant contribution from alkali-C_{60} optic phonons. Although the lack of a significant Rb isotope effect seems to rule out an alkali phonon contribution to pairing leading to a superconducting state, the small negative α_{Rb} could possibly be an artifact anharmonic alkali dopant potential in the interstitial sites. Whereas, we note that the value of α_{Rb} may hint at a similarity with the inverse hydrogen isotope effect in strongly anharmonic palladium hydride [13,14]. The reduced value of α_c imposes a constraint on the pairing mechanism of superconductivity in AMIF and raises the interesting possibility that alkali-C_{60} optic phonons may contribute to pairing, where alkali-metal isotope effect exponent may be masked by the effects of an anharmonic potential [11].

The widely debated issues in high T_c superconductors are the symmetry of the order parameter and the magnitude of the energy gap. It is generally believed that the AMIF holds *s*-wave symmetry of the order parameter [15]. Wide frequency scale of phonon modes, mediating a pair of electrons, is reflected in the magnitude of energy gap that varies from different spectroscopic techniques. On the other hand, point contact tunneling measurements predict a large energy gap ratio ($\beta = 2\Delta_0/k_BT_c$) of 5.2 ± 0.3 for Rb_3C_{60} in strong coupling regime [16]. Although tunneling measurements predict a large magnitude of the reduced energy gap, the BCS theory ($\beta = 3.53$) supports a low energy inter-molecular phonons as the source of superconductivity. However, several other reports on energy gap, i.e., far-IR measurement [17,18], muon spin relaxation measurement [19], and NMR measurement [20,21], provide a gap ratio ($\beta = 2\Delta_0/k_BT_c$) of 2.98 to 3.6 which is closer to BCS weak coupling limit, and absolute reflectivity data [22] provide energy gap value of $\beta = 2.98$ for Rb_3C_{60}. These values are close to those obtained from nuclear relaxation measurement [20]. The relaxation measurement in the normal state suggests that the coupling between the electrons and the low frequency phonons, i.e., inter-molecular phonons or radial intra-molecular phonons, is important for superconductivity in alkali metal-doped fullerenes Rb_3C_{60}. Optical transmission and tunneling studies [23], photoemission studies [24], and STM measurements [25] on Rb_3C_{60} led to $\beta = 4.2 \pm 0.2$, 4.1, and 5.3, indicating that the superconductivity cannot be described in the weak coupling limit. Although spectroscopic techniques [15-25] favor the electron–phonon coupling, they are unable to characterize phonons responsible for the pairing mechanism. Again limits for weak or strong coupling are also unpredictable.

Mechanisms for pairing in fullerides have been suggested in abundance. Zhang and coworkers first proposed that the doped alkali ion phonon mode produces a strong attraction for electrons on C_{60} using a Hubbard model to describe the superconductivity [26]. Varma et al. argued that the electron–phonon interaction in fulleride be induced by high frequency intra-molecular vibrational modes on a ball of C_{60}, and it should be a key feature of superconductivity [27]. Using quantum chemical calculations, it is argued that intra-molecular vibrations strongly scatter the electrons near Fermi surface, and modes near 1,428.0 and 1,575.0 cm^{-1} are strongly coupled. The electron–phonon coupling parameter (λ_{ra}) is evaluated as 0.11. It is likely that intra-molecular vibrations will lead to a superconducting state in fullerides [28].

Further, we note that Kresin analyzed the reported data on superconducting fullerenes based on generalized expression for T_c and argued that the strong electron vibrational coupling will describe the superconducting state. The accurate results reflected from the self-consistent approach for intra-molecular vibration [29,30]. However, the theory of Zhang and Guo led to the fact that the coupled Rb^+ optical mode and the vibration of C_{60} mass center will induce a strong electron–phonon interaction [31]. They have pointed that the value of electron–phonon coupling parameter for the intra-molecular vibrations is too small to explain the superconductivity. Ivanov and

Maruyama have proposed a three square well model which is characterized by windows of low-frequency inter-molecular phonons, high-frequency intra-molecular, and Coulomb energy; they find that these interactions allow a coherent interpretation of superconducting fulleride properties [32]. Furthermore, Alexandrov and Kabanov have developed a non-adiabatic theory of super-conductivity taking into account the polaron band narrowing and the realistic electron–phonon, as well the Coulomb interactions [33]. In these theoretical approaches, the main contribution to the transition temperature in fullerides is obtained by intra-molecular phonons, and indeed experimental reports for alkali isotope effect failed to show the possible participation of inter-molecular phonons.

Studies on transition temperature under high pressure are another convincing test for the characterization of participating phonon modes in the wide energy scale of phonon spectrum. In the AMIF, T_c monotonically changes with the unit cell size (lattice constant) a. The value of a can be varied in a number of ways. The pressure effect in fullerides is huge, dT_c/dP is negative, and the $dT_c/d\ln a$ ratios for different fullerides are close to each other. The direct measurements of the pressure dependence of the superconducting T_c for single-phase Rb_3C_{60} by Sparn and coworkers [34,35] revealed that T_c (=29.6 K) decreases strongly with increasing pressure, $dT_c/dP = -9.7$ K/GPa. Subsequently, measuring magnetic susceptibility [36] under hydrostatic pressure yields $dT_c/dP = -7.8$ K/GPa with a T_c of 19.3 K for K_3C_{60}. In the theory of Chaban, the dependence of T_c on the pressure is argued to be connected with the chemical pressure effect in fullerides [37]. The sensitivity of the pressure dependence of the T_c to the variations in T_c has been questioned to be an evidence of phonon pairing mechanism with either weak or strong coupling in AMIF. Finally, the reported universal increase of T_c with lattice parameter in high-pressure experiments has been invoked to support weak coupling theory with high frequency intra-molecular phonons.

In this respect, it is interesting to look at the nature of superconducting state to which the energy scale of the mediating boson in the electron-paring interaction is crucial in determining whether weak or strong coupling is appropriate. It is widely believed that the high frequency (approximately 400 to 1,400 cm^{-1}) intra-molecular modes or electronic excitation would tend to favor the weak coupling theory, while inter-molecular modes (approximately 15 to 150 cm^{-1}) would require normally strong coupling theory. This motivates us to seek a deeper understanding of the transition temperature and its pressure, as well as volume dependence, of fullerides taking into account of both inter-and intra-molecular phonons. In the fullerenes Rb_3C_{60}, the inter-molecular vibrations possess the energy in the range of 2 to 20 meV, and the band structure calculations have reported Fermi energy (ε_F) as 0.2 to approximately 0.3 eV [38].

In what follows, fullerides obey $\omega_{er} < \varepsilon_F$, so the consideration of inter-molecular vibrations, i.e., the coupling of the conduction electrons with the inter-molecular phonons, will be reasonable as a good starting point. In the problem of fullerides, we do believe that the coupling of conduction electrons with the displacements of C_{60} molecule or the alkali ions will induce the superconductivity. The coupling with the displacements of the alkali C_{60} optic is no doubt important to the electron–phonon interaction, because the isotope effects of C_{60} are present in the superconducting phase of Rb_3C_{60}. In the theory of Zhang and Guo, the coupling parameters are small for the intra-molecular vibrations to produce medium T_c [31]. We shall introduce the coupling of conduction electrons with the intra-molecular phonons in an *ad hoc* manner believing that our results are of importance. Nevertheless, this *ad hoc* interaction should provide sufficient extra coupling between conduction electrons as the energy scales for the frequency of this interaction would be much larger than the usual inter-molecular phonon frequency. Analyzing the isotope effect and pressure dependence of transition temperature will be a further test of the proposed idea.

In totality, the normal state resistivity measurements on AMIF reveal its metallic behavior. For polycrystalline films of Rb_xC_{60}, Kochanski et al. have first reported the resistivity measurement data as function of both temperature and doping (x) [39]. The minimum resistivity for Rb_3C_{60} film is about 2.2 m Ω cm near the Mott limit. Using a Fermi wave vector $k_F = 0.5$ $Å^{-1}$, together with minimum resistivity in the Boltzmann equation, would yield an electronic mean free path (ℓ) of 2.3 Å which is small in the metallic state. Subsequently, Palstra and coworkers have reported the measured longitudinal resistivity of thin films of Rb_3C_{60} in the normal and superconducting states in the magnetic fields up to 12.5 T [40]. The effective mean free path is found to be of the order of inter-atomic distances, the system being near metal-insulator transition. Xiang and coworkers [41] have first documented the resistivity measurement data of single crystal Rb_3C_{60}. The observed temperature dependence can be accounted for with an electron–phonon scattering mechanism if there is a high frequency contribution from the intra-ball phonons and a lower frequency contribution from phonons with frequencies in the range of 10 to approximately 100 cm^{-1}. The overall temperature dependence of $\rho(T)$ above T_c places constraints on the normal state transport models.

The magnetoresistance experiments on superconductive single crystal Rb_3C_{60} in fields up to 7.3 Tesla were reported [42]. The measurements yield superconducting state and normal state parameters, including upper critical field, coherence length, penetration depth, scattering time,

mean free path, and zero resistivity. They pointed that although their analysis assumes the metallic conduction, the relatively high normal state resistivity suggests the possibility of non-conventional scattering mechanisms. The temperature dependence of thermoelectric power of single crystal Rb_3C_{60} is reported by Morelli and is analyzed in terms of electron–phonon interaction [43]. It is noticed that the low temperature behavior is consistent with electron–phonon mass enhancement effects if it is assumed that the electrons are coupled strongly to low frequency inter-ball or ball alkali-metal atom phonons with effective energy $\theta^* = 185$ K.

Substantial progress has been made in analyzing the normal state resistivity of Rb_3C_{60} superconductors. A good fit to the temperature-dependent resistivity of Rb_3C_{60} can be obtained only by including a phonon mode with $\theta^* = 185$ K [44]. Gelfand and Lu have proposed a model for the electrons in the conduction band of alkali metal-doped C_{60} and suggested that the intrinsic orientation disorder might have a substantial influence on the electronic properties of these molecular materials [45]. Crespi et al. have analyzed the single crystal Rb_3C_{60} resistivity data using Ziman's resistivity formula from the view of electron–phonon coupling [46]. The analysis reveals that contributions from both high frequency intra-ball and low frequency inter-ball modes will be sufficient to account for the superconductivity.

Using parallel resistor extension to Bloch-Boltzmann theory, Hou et al. have pointed that high-temperature resistivity of single crystal Rb_3C_{60} does not show signs of resistivity saturation up to 800 K [47]. They successfully fit the resistivity data using the intra-molecular phonons with a frequency of $\omega_{ra} = 1{,}220$ K. Although the low frequency inter-ball phonons will be strongly temperature-dependent, the fit to the Ziman formula suggests that the coupling to these modes is small. The normal state resistivity measurement [39-47] points to the fact that apart from both on-ball molecule vibrations and alkali C_{60}, optic phonons and electron–electron interactions in the metallic state are important in retrieving the measured data. However, it is not clear that the normal state resistivity minima will correspond to inter- or intra-molecular phonons.

Observing various experimental reports [1-25,34-38] and theoretical proposals [26-33], we have made our efforts to reveal the nature of pairing mechanism and physical properties leading to superconducting state by considering the three-dimensional (3D) Rb_3C_{60} as a diatomic lattice with C_{60} molecule and alkali metal (Rb) ions. We first provide technical details and motivate them by simple physical arguments before summarizing our main findings. In a true sense, the rotation of C_{60} molecule is almost completely inhibited below 250 K and hence need not be included in a theory dealing with the system at temperature near the transition temperature of fullerides. Furthermore, the molecular vibrations of fullerides in three-dimensional network are quite complicated because the Coulomb interactions between bond charges of covalent bond belong to different molecules. For the requirements of consistency, the lattice parameter (a) and Bulk modulus (B) are used from experiments to derive the force constant (κ) and the longitudinal phonon modes propagating along 110 direction, which are due to the displacement of C_{60} molecule and alkali ions. We use the inter-molecular optical phonon frequency of Rb_3C_{60} to estimate the superconducting transition temperature, in the strong coupling theory of superconductivity. Later on, the intra-molecular phonons are introduced to obtain an analytical result on transition temperature, carbon isotope exponent, the energy gap ratio, and the pressure and volume effect on transition temperature. It is the purpose of this investigation to determine the relative contributions of these vibrations in pairing, assuming that they coexist. Note that we shall present our results in terms of s-wave pairing state.

We have further devoted our efforts to interpret the temperature-dependent resistivity of single crystal Rb_3C_{60} data. Our emphasis is to first see the relative strength of coupling strengths for inter- and intra-molecular vibrations. Later on, the role of the electron–electron interactions is explored. We are not going to make any exception and will also deduce the resistivity within the framework of Bloch-Gruneisen theory. We will show the resistivity as obtained from the electron–phonon-coupling strength using the McMillan-Hopfield parameter for real space formulation and the density of states at the Fermi level for estimating coupling strength. The objective is to characterize phonon modes which best reproduce the form of temperature-dependent resistivity and play a major role in pairing mechanism.

This paper is arranged as follows. In “The model” section, we first derive the force constants and the longitudinal phonon frequency for C_{60} molecule. Furthermore, a relationship between force constant for undoped and alkali metal-doped fullerenes has been established. The longitudinal phonon modes of Rb_3C_{60} propagating along 110 directions are evaluated. The effective coupling strength between the conduction is then deduced, and renormalized Coulomb repulsive parameter for the inter-molecular phonon frequency (ω_{er}) is used to estimate T_c^{er}. In the next step, the intra-molecular phonons are used for the estimations of T_c. In order to test the validity of the above approach, the carbon isotope effect, the reduced energy gap parameter, the pressure and volume effect on T_c, the thermodynamical parameters describing the superconducting state, and normal state resistivity for Rb_3C_{60} are also estimated. The details of numerical analysis are presented along with discussions in the ‘Results and

discussion' section. The purpose of the present investigation is to improve the understanding of various physical properties by including the effects of Coulomb and inter- and intra-molecular phonons. However, we do not claim the process to be rigorous, but the results we report here do indeed throw light on the nature of these interactions in the test material. Conclusions are discussed in the last section where we provide physical descriptions of the model calculations involved.

The model

The undoped C_{60} molecule is a pure carbon compound and possesses a spherical structure. The nuclear cage of C_{60} (the C_{60} sphere) has the following diameters: 7.1 Å with two-bond length (6–6 ring), 1.4 Å, and 1.46 Å (6–5 ring). The distance of the nearest approach in the molecular solid is 3.1 Å [48]. The C_{60} molecule crystallizes in the *fcc* phase with lattice parameter $a = 14.20$ Å, and the distance between the centers of the nearest neighbor C_{60} cages is $b = a/\sqrt{2}$. Furthermore, in C_{60} molecule, out of four valence electrons on each carbon atom, three electrons participate in the 90 σ bonds along the edges of truncated isocahedron, and the remaining 60 electrons of the molecule are in the orbitals.

In fact, the diameter of C_{60} molecule is large in such a way that the electron density is localized near the surface of the sphere. Electronic energy band structure reveals that for C_{60}, the lowest unoccupied molecular orbital is empty and can accommodate six electrons [49,50]. The C_{60} cages may be regarded as rigid spheres, and a bandwidth develops from the weak interactions between the nearest neighbor (n-n) C_{60} cages. In the following, the n-n C_{60} cage interactions are first considered, and the force constants along with the phonon frequencies of the *fcc* lattice are then derived.

To begin with, consider the undoped C_{60} molecule as a cube with N cages, and volume is $Na^3/4$. When the volume is compressed from V to $V + dV$, the work done is

$$W = (B/2)\left(\frac{\partial V}{V}\right)\partial V = \frac{B(\partial V)^2}{2V}, \tag{1}$$

B being the Bulk modulus and a is the lattice parameter. For a cube, $V = a^3$ and $\partial V/V = 3\partial a/a$. Keeping in mind the contribution of $6N$ bonds between n-n C_{60} cages, W is expressed as

$$W = \frac{3N}{k\left[\frac{\partial a}{\sqrt{2}}\right]^2}, \tag{2}$$

where κ is the force constant for n-n cages. A comparison yields $\kappa = 3Ba/4$. A set of C_{60} molecule is treated as a three-dimensional monoatomic lattice with atomic mass and the position of cage as m_k and $u\binom{l}{k}$, respectively. The lattice considered S unit cells numbered by an index $l = 1,2\ldots S$ and for masses k (=1) [51]. The equations of motion along 110-direction are obtained from force $-\partial\Phi/\partial u\binom{l}{k}$ acting on the atom $(_k)$ with Φ as the potential energy of the crystal and follows

$$-m_k u_j(k) = K\left[2u_j(k) - u_{j+1}(k) - u_{j-1}(k)\right] \tag{3}$$

also

$$-mu_j(l) = k\left[2u_j(l) - u_{j+1}(l) - u_{j-1}(l)\right] \tag{4}$$

The equilibrium position of the lth unit cell relative to an origin located at some atom is $r(l) = l_1\ a + l_2\ b + l_3\ c$, where l_1, l_2, and l_3 are integers and a, b, and c are the primitive translational vectors. Using the plane wave solution as $u_j(l) = A(q)\exp i[q_j r(l) - \omega t]$, with A as the amplitude, q is the wave-vector in 110 direction, and $\omega(q)$ is the angular frequency, the dispersion relation reads

$$\omega_L(q) = 2\sqrt{k/m} = \sqrt{\frac{3Ba}{m}} \tag{5}$$

at the zone boundary ($q = \pi/b$). The above is the longitudinal phonon mode, which is due to the rotational motion of the C_{60} molecule. The lattice is expanded due to intercalation of K, Rb, and Cs at tetrahedral and octahedral sites when C_{60} molecule is doped; this is discussed in the following subsection.

The C_{60} molecule when chemically substituted with alkali metal (Rb) atoms becomes metallic at the Rb_3C_{60} composition, and it shows the superconducting nature. With the doping, Rb atoms become fully ionized in the C_{60} crystal and give up their electrons to highly polarizable C_{60} molecule. These electrons go to the delocalized lowest unoccupied molecular orbitals, which can accommodate six electrons. The conduction band is empty for C_{60} crystal, and for Rb_3C_{60}, the conduction band is half filled up to the Fermi level. The Rb atoms were located in two non-equivalent tetrahedrals and an octahedral position of the lattice. In doped fullerides, there exists 6 N C_{60}-C_{60} bonds at a bond distance of $a/\sqrt{2}$ and 8 N C_{60}-Rb bonds with bond distance as $a\sqrt{3}/4$ with $a = 14.45$ Å for Rb_3C_{60}. In the true sense, a dopant entering in to parent lattice C_{60} tends to expand the lattice to create a place for itself.

The transfer of charge will certainly result in to some contraction, and the final lattice parameter of the doped material will be resultant of these effects. It is noticed that the lattice parameters for K_3C_{60} ($a = 14.28$ Å), Rb_3C_{60} ($a = 14.45$ Å), and Cs_3C_{60} ($a = 14.60$ Å) which are more than the lattice parameter of undoped C_{60} namely $a = 14.20$ Å and, hence, there is a resultant

expansion [1-3]. Furthermore, out of the 8 N C_{60}-Rb bonds, four N are at octahedral position, and four N take the tetrahedral position. For the sake of simplicity, the Rb atoms are considered at the tetrahedral site, as the cavity is large enough to accommodate Rb atom. The total bond energy within the harmonic approximation is expressed as

$$E_B = \frac{6Nk}{2\left[\left(a/\sqrt{2}\right) - r_{CC}\right]^2} + \frac{8Nk'}{2\left[\left(\frac{a\sqrt{3}}{4}\right) - r_{MC}\right]^2}, \qquad (6)$$

where r_{CC} is the equilibrium C_{60}-C_{60} bond distance (10.04 Å) and r_{MC} denotes the metal-C_{60} bond distance and is $r_{MC} = (r_{CC}/2) + r_i$, with $r_i = 1.48$ Å is the ionic radius of Rb. A relationship between the force constants κ (C_{60}-C_{60}) and κ' (M-C_{60}) is established when the total bond energy reaches its maximum at the experimental value of lattice parameter a.

Let us now consider the n-n interactions between the C_{60} cages and C_{60} cages bonded to both Rb atoms as well as the adjacent C_{60} cages while the Rb atoms are bonded to C_{60} cages only. Treating Rb_3C_{60} as a three-dimensional diatomic lattice with atomic masses as m (M) and positions u (v) for C_{60} (Rb), the equations of motion follows

$$-mu_j(l) = k\left[2u_j(l) - u_{j+1}(l) - u_{j-1}(l)\right] + 2k_1\left[2u_j(l) - v_{j+\frac{1}{2}}(l) - v_{j-\frac{1}{2}}(l)\right] \qquad (7)$$

$$-Mv_j(l) = k_1\left[2v_j(l) - u_{j+\frac{1}{2}}(l) - u_{j-\frac{1}{2}}(l)\right] \qquad (8)$$

The plane wave solutions are used as $u_j(l) = A \exp i[q_j\, r(l) - \omega t]$ and $v_j(l) = B \exp i\,[q_j\, r(l) - \omega t]$ and $\kappa_1 = 0.66\,\kappa'$. It is useful to expand the coefficient Φ, i.e., the atomic force constants about its equilibrium value using the 3D forms of Taylor theorem for small displacements. Following harmonic approximation, all cubic and higher order terms are neglected. Also, the nearest neighbor interactions naturally demand the force constants and several other parameters in 3D. For various symmetries in Rb_3C_{60}, several transverse and longitudinal frequencies will be then obtained from the 3D dynamical matrix and are rigorous which indeed is not included in the scope of the present analysis. Confining only for the longitudinal phonon modes of Rb_3C_{60} along 110-direction, the dispersion relation reads for small q value

$$\omega_+^2 = 4\,[D_1 + D_2] - \frac{D_1 D_2}{[D_1 + D_2]\,(qb)^2} \qquad (9)$$

$$\omega_-^2 = \frac{D_1 D_2}{D_1 + D_2}(qb)^2 \qquad (10)$$

Here, $D_1 = [\kappa + (2\kappa'/3)]m^{-1}$ and $D_2 = [\kappa'/3]\,M^{-1}$. Equation (9) is an inter-molecular optical mode, and the acoustic characteristics are seen from Equation (10) in the long-wavelength limit ($q \to 0$). The developed phonon modes are due to the displacement of C_{60} molecule or Rb^+ ions in the Rb_3C_{60}. Initially, the coupling of conduction electrons with the inter-molecular optical vibrations (ω_+) is considered and is believed to provide the attractive force for superconductivity in fullerides. As an application, the coupling parameters of Rb_3C_{60} are evaluated in the following subsection.

The evaluation of superconducting transition temperature indeed needs the information about the attractive electron–phonon coupling strength and the Coulomb repulsive parameter. Generally, the phonon-mediated interaction is usually treated first, and then direct Coulomb interaction is introduced in terms of pseudopotential, μ^* [52-56]. The estimation of T_c concentrates on treating the phonon-mediated interaction in the strong coupling theory with great accuracy, while the Coulomb interactions μ^* along with the electron–phonon coupling constant λ are often incorporated in an approximate way. In dealing with a high-T_c superconductor, it is more realistic to first consider the large electron–electron interaction and later the small electron–phonon interaction strength to estimate T_c.

The effect of screening of electrons is determined by the renormalized Coulomb repulsive parameter as [52,53]

$$\mu^* = \frac{\mu}{\left[1 + \mu \ln\left(\varepsilon_F/\omega_{er}\right)\right]}, \qquad (11)$$

where the cut-off frequency is set equal to the inter-molecular optical phonon frequency. Usually, the Coulomb repulsive parameter μ is obtained in terms of Fermi wavevector k_F and the Thomas-Fermi wavevector (k_s) as

$$\mu = \chi^2 \ln\left[\left(1+\chi^2\right)/\chi^2\right] \qquad (12)$$

Here, the abbreviation $\chi^2 = k_s^2/4k_F^2$ and $k_s^2 = 6\pi ne^2/\varepsilon_\infty\, \varepsilon_F$. The density of electrons is n, with ε_∞ being the high frequency dielectric constant and ε_F is the Fermi energy.

Superconducting tunneling data yields the electron–phonon spectral weight $\alpha^2 F(\omega)$ from a strong coupling inversion procedure for the estimation of the coupling constant. On the other hand, the attractive coupling constant can be calculated from the McMillan formulae [57] which are related through the density of states at Fermi level $N(0)$ and the mean square electron-ion matrix. Band structure calculation of Rb_3C_{60} using full potential linear muffin-tin orbital [58] method suggests that the superconducting electrons are composed entirely of carbon $2p$, the contribution of C $2s$ orbital is very small, and the largest contributions to $N(0)$ are provided by the C (3) atoms which are the closest to the neighboring C_{60} molecule. The density of states is larger than that of ordinary metals. The use of McMillan

expression is appropriate in Rb_3C_{60} superconductors for twofold reasons: large density of states and the larger mass difference of Rb and C_{60}. The electron–phonon coupling strength λ is

$$\lambda = \frac{N(\varepsilon_F) < I^2 >}{M < \omega^2 >}, \tag{13}$$

where $< I^2 >$ is a mean square electron-ion matrix element, M the molecular mass, and $< \omega^2 >$ is an averaged square molecular vibration frequency.

The mean square electron-ion matrix element is

$$\begin{aligned} < I^2 > = & \left\{ \left[\Omega/(2\pi)^3\right]^2 \int d^3k \int d^3k' (k-k')^2 \right. \\ & \left. |V(k-k')|^2 \, \delta(E_k - \varepsilon_F) \delta\left(E'_k - \varepsilon_F\right) \right\} \\ & \left\{ \left[\Omega/(2\pi)^3\right]^2 \int d^3k \int d^3k' (k-k')^2 \right. \\ & \left. \delta(E_k - \varepsilon_F) \delta\left(E'_k - \varepsilon_F\right) \right\}^{-1} \end{aligned} \tag{14}$$

$$\begin{aligned} & = \left\{ \left[N \, \varepsilon_F\right]^2 \int_0^{2k_f} (q dq / 2k_F^2) \, q^2 |V(q)|^2 \right\} \\ & \quad \left\{ \left[N \, \varepsilon_F\right]^2 \int_0^{2k_f} (q dq / 2k_F^2) \right\}^{-1} \\ & = \int_0^{2k_f} q^3 dq |V(q)| / \int_0^{2k_f} q dq, \end{aligned} \tag{15}$$

where, $V(q)$ is the screened Coulomb potential. In terms of bare Coulomb potential $V_c(q)$ one expresses, $V(q) = V_c(q)/\varepsilon(q)$. The dielectric function $\varepsilon(q,\omega)$ is

$$\varepsilon(q,\omega) = 1 + \omega_p^2 \left[\left(\frac{q^2 v_F^2}{2} \right) - \omega^2 \right]^{-1}, \tag{16}$$

where v_F as the Fermi velocity.

The static dielectric function $\varepsilon(q)$ in the long-wavelength limit is

$$\varepsilon(q) \approx \frac{4me^2 k_F}{\pi \hbar^2 q^2} \tag{17}$$

and the result for screened Coulomb potential is

$$V(q) = \frac{\frac{4\pi Z e^2}{q^2 \Omega}}{\frac{4me^2 k_F}{\pi \hbar^2 q^2}} \tag{18}$$

$$= \frac{\hbar^2 \pi^2 Z}{m k_F \Omega'} \tag{19}$$

where Ω is the volume of the cell and Ze denotes effective nuclear charge and is 7e.

Thus, the mean square electron ion matrix element from Equation (15) follows

$$< I^2 > = \left(\frac{\hbar^2 \pi^2 Z}{m k_F \Omega} \right) \int_0^{2k_F} q^3 dq / 2k_F^2, \tag{20}$$

and the electron–phonon coupling strength for the inter-molecular vibration frequency $< \omega_{er}^2 >$ is

$$\lambda_{er} = \frac{2N(\varepsilon_F) \left[\frac{\hbar^2 \pi^2 Z}{m\Omega} \right]^2}{M < \omega_{er}^2 >} \tag{21}$$

The values of the renormalized Coulomb repulsive parameter and the attractive electron–phonon coupling constant are used while estimating the superconducting and normal state parameters.

In the next section, we shall estimate the superconducting and normal state properties for alkali metal intercalated fullerenes Rb_3C_{60} namely: transition temperature T_c, the Carbon isotope effect α, the energy gap ratio β, the pressure and volume effect on T_c, and the thermodynamical properties describing the superconducting state, as well as the normal state resistivity and associated transport parameters for alkali metal intercalated fullerides.

Results and discussion

For the estimation of the superconducting state parameters of alkali metal intercalated Rb_3C_{60}, the realistic values of some physical parameters employed are as follows: the C_{60} molecule is first analyzed using the lattice parameter $a = 14.20$ Å and $B = 18$ GPa [59,60]. The effective mass of C_{60} cage is 1.2×10^{-24} kg, and the force constant κ is obtained as 19.17 N/m. The estimated value of the longitudinal phonon frequency of C_{60} molecule from Equation (5) is 42.40 cm^{-1} (5.2 meV). It is worth to mention that this phonon mode comes from six N bonds between n-n cages of C_{60} molecule.

Essentially, the rotation of C_{60} molecule is inhibited at temperatures near to room temperature, and it appears appropriate to ignore the rotation of C_{60} molecule in a theory dealing with system at temperatures in the vicinity of T_c. Chemical substitution of alkali metal ion in C_{60} molecule introduces extra electrons which are accommodated in the conduction band which is half filled up to the Fermi level, and these conduction electrons distort the lattice of Rb_3C_{60}. The distortion leads to a net expansion as lattice parameter for Rb-doped fulleride (14.45 Å), and parent fulleride is $a = 14.20$ Å. For the evaluation of force constant relationship, the total bond energy is then minimized at the experimental value of a (=14.45 Å) for Rb_3C_{60} to obtain κ' as 1κ. It appears

that the magnitude of force constant for alkali metal intercalated fullerenes is larger than the undoped C_{60}.

The dispersion relations for the inter-molecular phonon modes originate due to the displacement of C_{60} molecule, and Rb^+ ions are then obtained. It is evident from the eigen-frequencies that these correspond to the inter-molecular acoustic and alkali C_{60} optical modes in the long-wavelength limit ($q \to 0$). The mass of the three alkali metals (Rb) are used as 366.92 amu. The inter-molecular alkali C_{60} optic mode (ω_{er}) is obtained as 8.19 meV at $q \to 0$. The scattering of charge carriers at the Fermi surface is considered for all possible values of scattering angle θ. The wave vector q ($\cong 2k_F \sin\theta$) can therefore takes maximum value up to $2k_F$. For small value of q, the product qb is 10 to deduce the value of acoustic mode as 105 meV at $2k_F$. The electron density n ($=4 \times 3/a^3$) is estimated at 4×10^{21} cm^{-3} from the lattice parameter a of Rb_3C_{60}, and the band structure value of mass as 3.6 m_e is used [58].

The Fermi energy is obtained as 0.25 eV which is consistent with the earlier data, $\varepsilon_F = 0.2$ to approximately 0.3 eV [4,5,38]. The other parameters of the electrons are the screening parameter k_s ($\cong$ 0.99 Å^{-1}) and the Fermi wave vector k_F ($\cong$ 0.49 Å^{-1}) which are required for the determination of the Coulomb repulsive parameter. We have used the value of ε_∞ as 4.4 [61]. The renormalized Coulomb repulsive parameter μ^* is estimated at 0.21 and is attributed to the fact that ε_F is higher by at least an order of magnitude with the inter-molecular alkali C_{60} optic phonon frequency. The electron–phonon coupling strength (λ_{er}) using Equation (21) is obtained as 1.17. We note that the dimensionless electron–phonon coupling strength as estimated by Gunnarson is about 0.5 to 1 [4,5]. Generally, the moderately large value of Coulomb repulsive parameter is appropriate for a narrow bandwidth material on the metallic side of a metal-insulator transition. To this end, one can see that in dealing with Rb_3C_{60} fullerides, the coupling strength ($\lambda > 1$) and the renormalized Coulomb repulsive parameter ($\mu^* = 0.21$) for the characteristic phonon frequency ($\omega_{er} = 8.19$ meV) are believed to distort the lattice, leading to a superconducting state. We begin by analyzing the superconducting transition temperature.

In the regime $\lambda > 1$, the strong coupling theory applies and the transition temperature T_c for Rb_3C_{60} is estimated following [62]

$$T_c^{er} = 0.25\omega_{er}\left[\exp\left(2/\lambda_{eff}\right) - 1\right]^{-\frac{1}{2}}, \quad (22)$$

where

$$\lambda_{eff} = (\lambda_{er} - \mu^*)[1 + 2\mu^* + \lambda_{er}\mu^* t(\lambda)]^{-1} \quad (23)$$

and

$$t(\lambda_{er}) = 1.5\exp(-0.28\lambda_{er}). \quad (24)$$

The effective coupling constant λ_{eff} is deduced as 0.57 for the numerical function $t(\lambda)$ value 1.08 with $\lambda_{er} = 1.17$ and T_c^{er} is estimated as $\cong$ 4.17 K which is much lower than the reported experimental data [1-3,34,35] of about 29.6 K. The low value of T_c is due to the fact that the vibrations developed due to the lattice deformations, i.e., the soft optical inter-molecular phonons, are considered. The above approach with inter-molecular phonons does not explain a medium T_c in Rb_3C_{60}; hence, it is important to look for the role of intra-molecular phonons to assess the reported value.

The role of collective excitation mechanism over conventional phonon mechanism in cuprates was earlier successfully explained with a generalized expression for T_c in a strong coupling theory [62]. A related problem is that whether one can utilize the broad vibrational spectrum of fullerenes for evaluating T_c or not. With this idea, an analytic result for T_c is obtained by incorporating the simultaneous presence of both inter- and intra-molecular phonons in fullerides using

$$T_c = T_c^{er}\left[\omega_{ra}/T_c^{er}\right]^{\Lambda}, \quad (25)$$

where

$$\Lambda = \frac{\lambda_{ra}}{\lambda_{ra} + \lambda_{er}}, \quad (26)$$

λ_{ra} being the intra-molecular coupling constant and is obtained as 0.7 from the scattering time ($\tau = 0.8 \times 10^{-14}$ s) which is derived in the latter section while estimating the zero limited resistivity as

$$\lambda_{ra} = \frac{\hbar}{2\pi k_B T\tau}. \quad (27)$$

We have used the reported value of $\omega_{ra} = 847.9$ cm^{-1} from the earlier data [1-3]; T_c is obtained as 34 K. Hence, with the cooperative inter- and intra-molecular phonon mechanisms, the high T_c value in fullerides is explained. Although the intra-molecular phonons are incorporated in an *ad hoc* manner, it is believed that this approach will reveal the vibrational modes responsible for superconducting pairing in AMIF as well as the relative strengths of these couplings. The strength of coupling $\sigma = \lambda_{er} \setminus \lambda_{ra}$ is 1.67. From the analysis of superconducting T_c, it is natural to make two comments: (a) the high-energy intra-molecular phonons are moderately coupled while to that of the low-energy inter-molecular phonons are strongly coupled to neighboring electrons, and (b) T_c mainly arises from the significant contribution of intra-molecular phonons.

We now switch to the discussion of screening effects. It is widely believed that for conventional superconductors, retardation effects in view of different energy scales for electrons and phonons drastically reduce the effects of Coulomb interactions. In what follows, the dimensionless Coulomb repulsive parameter μ^* is therefore believed to severely reduce and, attributed to the scaling factor, ln $[\varepsilon_F/\omega_b]$ appeared in the denominator of the expression of μ^*. As the Fermi energy is larger, at least an order of magnitude by inter-molecular phonons, the retardation effects are expected to be very small. On the other hand, the Fermi energy and intra-molecular phonon frequency are of almost similar order, and hence vertex correction becomes important because the Migdal theorem does not hold and the frequency dependence of the effective Coulomb interaction should be considered in fullerides. The above issue will be addressed in future investigation by considering the Coulomb interactions more carefully. Generally, energy ω_b is presented as characterizing bosons (ω_{er} or ω_{ra}), but opinion about its choice in screening is far from being unanimous. The only thing one must be sure of is that, if a boson is a candidate for superconductivity, one must expect $\mu^* < \mu \sim 0.5$ and of course $\lambda - \mu^* > 0$. The importance of non-adiabatic effects in fullerides has been discussed at great length [63-65].

To obtain some specific results, we obtain numerical values for the transition temperature where coupling parameters are determined and presented in the following plots for various conditions. In Figure 1, we show the result for T_c as a function of μ up to 0.3 for a set of parameters $\lambda_{er} = 1.17$ and $\lambda_{ra} = 0.7$. The analytic expression for T_c from Equation (22) clearly demonstrates that T_c is strongly influenced by the Coulomb repulsive parameter and is higher for small values of μ. For a set of coupling parameters $\mu^* = 0.21$, $\lambda_{er} = 1.17$, and $\lambda_{ra} = 0.7$, a T_c of 34 K is estimated. Now, if we use the enhanced value of μ, it leads to enhanced μ^* accordingly. The net result is that the increased electron–electron repulsive contribution along with the inter- and intra-molecular phonons producing an attractive interaction is reduced against the phonon attraction alone and attributes to suppress T_c. The present study is essentially based on the application of strong coupling theory with an additional pairing force; we have the feeling that such studies describe the dependence of T_c on different coupling strengths, which has not been tested carefully and is definitive to impose any constraints on theoretical approaches.

It is clearly of interest to shed further light on various coupling strengths. An important feature of Equation (22) is displayed in Figure 2. We plot T_c as a function of λ_{er} up to 2.0 for a set of parameters $\mu^* = 0.21$ and $\lambda_{ra} = 0.7$. It is noticed from the curve that T_c increases initially with the enhanced value of λ_{er}. For the above set of parameters, if the present system is strongly coupled,

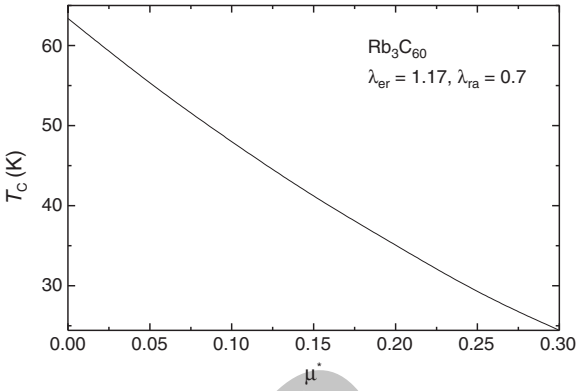

Figure 1 Variation of T_c as a function of μ^*.

then one can achieve the higher values of T_c. The values of coupling parameters as λ_{er} (=1.17), λ_{ra} (=0.7), and μ^* (=0.21) are quite reasonable in view of fulleride superconductors. We also investigate the effect of the intra-molecular phonon coupling strength on T_c. Figure 3 shows the variation of T_c for different values of $\lambda_{ra,}$ varying from 0.0 to 0.7. In plotting this curve, we take $\lambda_{er} = 1.17$ and $\mu^* = 0.21$. We see from this graph that T_c is highly sensitive to λ_{ra} even for moderate coupling. It is worth to comment that if we start with a pure inter-molecular phonon mechanism and later on add a correction term with moderately coupled intra-molecular phonons, then in this situation, one can easily enhance T_c values. Even though, in the present model, we have introduced an attractive intra-molecular phonon term in an *ad hoc* way, we, therefore, do not claim to possess a rigorous result for the coupling strength parameters. However, the essence of intra-molecular phonons can be further verified to see whether by this way one can enhance T_c and does the inter-molecular phonons play a crucial role in the attractive pairing mechanism.

We now focus on the relationship between λ_{er} and μ^* within the present formalism for Rb_3C_{60} superconductors.

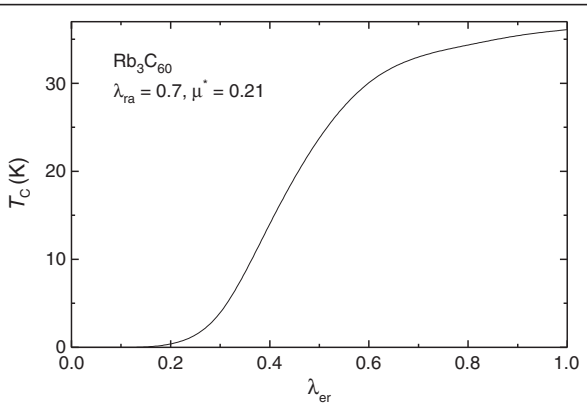

Figure 2 Variation of T_c as a function of λ_{er}.

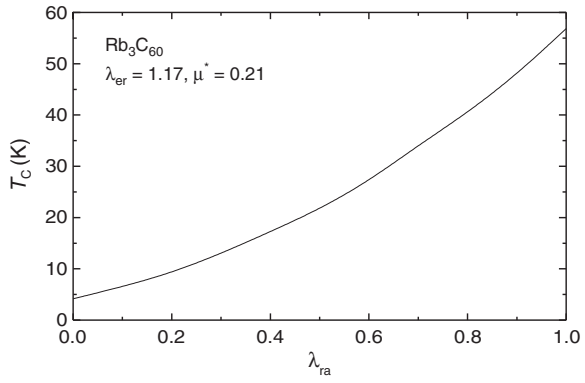

Figure 3 Variations of T_c for different values of λ_{ra}.

We plot the variation of λ_{er} with μ^* in Figure 4. For lower values of λ_{er}, μ^* yields unphysical values for a set of parameters ($T_c = 34$ K and $\lambda_{ra} = 0.7$). We expect that within the present approach, the inter-molecular phonons must be strongly coupled. Higher and positive μ^* implies a constant repulsive interaction that is insufficient to create a superconducting state despite of the additional coupling of intra-molecular phonons apart from electron-intermolecular phonon interactions. Correct picture of renormalized Coulomb repulsive parameter is reflected in these fullerides with intermediate electron-intra-molecular phonon coupling. We end up by arguing that even if we include the intermediate coupling of intra-molecular phonon, the result for μ^* is affected by λ_{er} in a usual way and is consistent with the conventional superconductors.

Given the transition temperature, we proceed to calculate and discuss the carbon isotope effect coefficient. The isotope effect coefficient is

$$\alpha = (0.5)\left(\frac{d\ln Tc}{d\ln\omega}\right). \tag{28}$$

From Equations (22) and (28), the ω dependence of T_c is introduced in terms of μ^* following the relation $\mu^* d\ln\omega = d\ln\mu$; this leads to the following result of isotope effect coefficient as

$$\alpha = \frac{\left\{1 - \frac{\mu^{*2}\left(1+2\lambda_{er}+\lambda_{er}^2\right)}{\lambda_{eff}(\lambda_{er}-\mu*)\left[1+\left(\frac{4T_c}{\omega}\right)^2\right]}\right\}}{2}, \tag{29}$$

where ω is the average phonon frequency. The mass of carbon directly influences the inter-molecular phonon frequency, as $\omega_{er} \sim [m\ M/(m+M)]^{1/2}$ with m (M) mass of C_{60} (K) and a finite value of isotope effect is expected. Equation (29) yields $\alpha \cong -0.09$ which is slightly lower than the reported value of $\alpha = -0.028 \pm 0.036$, a result that implies that the inter-molecular optical phonon plays at most a minor role [12] and consistent with the results [11]. A shift in T_c is an indication of an important role of coupling of the conduction electrons with the displacement of C_{60} molecule or alkali ions. The reduced inter-fullerene mass $[mM/(m+M)]$ is definitely small in comparison with the intra-fullerene mass $[(m+M)/2]$. The carbon isotope exponent essentially causes the change in inter-molecular phonon frequency; thus, it is argued that although intra-molecular phonons do play a significant role, the participation of inter-molecular phonons cannot be ignored. Figure 5 shows the variation of estimated isotope effect from Equation (29) with screening parameter. It is noticed that the BCS one-half value is recovered for $\mu^* = 0.0$. With the increase in μ^* values, the isotope effect exponent decreases for $\lambda_{er} = 1.17$ and $\lambda_{ra} = 0.7$. In order to assess further the role of electron–phonon in the pairing mechanism, we require the total isotope effect.

However, a reliable alkali metal isotope effect is not reported for Rb_3C_{60} system, but a negative α_{Rb} is documented that necessarily ruled out the possibility of participation of inter-molecular phonon [12]. We expect that the requirement is to know whether the ratio α_c/α_{Rb} or the total isotope effect has a final conclusion about the role of inter- or intra-molecular phonons in the

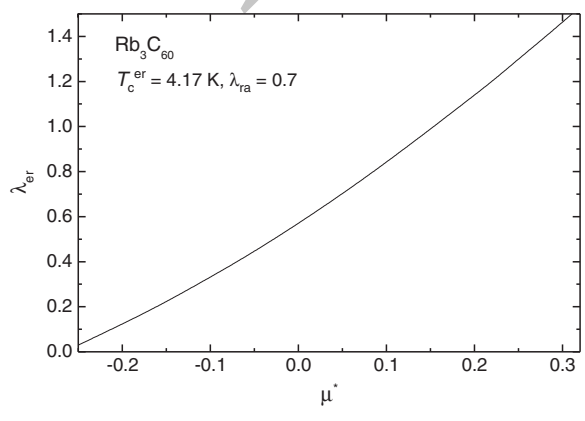

Figure 4 Variations of λ_{er} with μ^*.

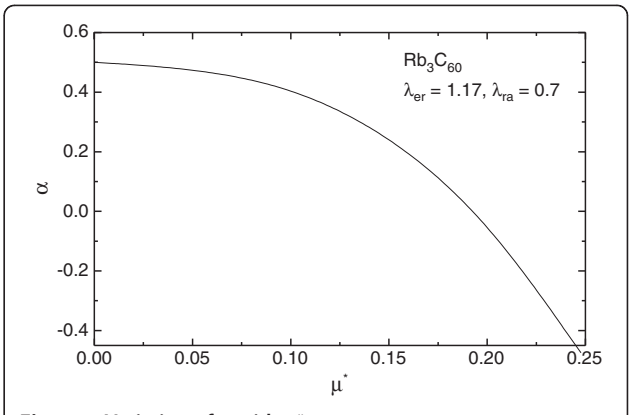

Figure 5 Variation of α with μ^*.

superconducting state. The justification lies in the fact that the ratio α_c/α_{Rb} depends on the weights of on-ball carbon and carbon alkali metal-dominated phonon modes that are sensitive to λ and μ^*. We further expect that the Coulomb interactions, multi-atomic compounds, anharmonicity, and non-phonon mechanisms may affect the value of isotope effect exponent and will be investigated in near future.

As a next step, we focus on the magnitude of the energy gap parameter as the wide energy scale of phonons essentially points either weak or strong coupling in AMIF. The energy gap parameter β is [29,30]

$$\beta \cong 2\Delta(0)/k_B T_c = 3.52\left[1 + 5.3(T_c/\omega)^2 \ln(\omega/T_c)\right] \quad (30)$$

where $\Delta(0)$ is the energy gap at zero temperature. The energy gap parameter provides a measurement of coupling strength for phonon-mediated electron–electron interaction. Substantial doubts arise on tunneling measurement data [16] which predict significantly higher values of β in Rb_3C_{60} fullerides. It is therefore of interest to address this issue.

The energy gap parameter ($\beta \cong 3.6$) is estimated using ω_{er} as 60.025 cm^{-1} and T_c of about 4.17 K from Equation (30). The magnitude of energy gap is higher than the BCS limit of 3.53 and thus indicates the strong coupling regime. On the other hand, the gap parameter when intra-molecular phonons are considered in the pairing mechanism, is estimated as 3.57 which is close to the BCS limit where the values ω_{ra} = 847.9 cm^{-1} and T_c = 34 K are used. This implies that the intra-molecular phonons require weak interactions with the conduction electrons and is consistent with the infrared spectroscopy [17,18], muon spin relaxation rate measurements [19], and nuclear spin relaxation measurements [20] which strongly favor the participation of intra-molecular phonons in the pairing mechanism. Furthermore, the absolute reflectivity measurements [22] and STM measurements [25] on Rb_3C_{60} report $\beta = 3$ to approximately 5.0, which are higher than the BCS weak coupling limit, and the electron–phonon coupling strength cannot be as large as 2. Thus, one cannot escape stating that the low-frequency intermolecular phonons are strongly coupled, while the high-frequency intra-molecular phonons are weakly coupled. There exists an uncertainty about the energy gap value in Rb_3C_{60} and from its reduced value; the relative strength of inter- as well as intra-molecular phonons is well understood.

We now devote our efforts to reveal several thermodynamical parameters describing the superconducting state in next subsection. Generally, various thermodynamical parameters describing the superconducting state of a superconductor, for instance the Ginzburg-Landau parameters, the lower and upper critical magnetic field, average value of critical magnetic field and the temperature derivative of the upper critical magnetic field, can be very well estimated by knowing λ_L and ξ values and are of great importance. The present calculations reveal a Fermi velocity v_F ($\cong 1.6 \times 10^7$ cm s^{-1}) relative to the reported value from LDA electronic structure calculation for Rb_3C_{60} (1.6×10^7 cm s^{-1}) [49,50]. A consistent value of v_F along with a T_c of 34 K leads to a BCS coherence length of 6.5 nm using the precise definition $\xi(0) \cong \hbar v_F/1.76\pi k_B T_c$ which is consistent with reported value of 4.0 to approximately 5.5 [44]. The Pippard coherence length in the clean limit is an intrinsic parameter, and the not-sensitive-to-material properties is related to ξ_0 by the relation $\xi_0 \simeq [\xi(0)\ell]^{1/2}$. Here, we use the value ξ_0 = 2.86 nm which is consistent with the reported data of 2.0 nm [34,35,44], 3.0 nm [66], and 2 + 0.3, 2–0.2 [34,35] for Rb_3C_{60} fullerenes.

It is interesting to comment that the coherence length which, even if small, is much larger than the inverse Fermi momentum. We further estimate the zero temperature mean free path, $\ell = v_F\tau \approx 1.28$ nm which is consistent with the reported value of 0.9 nm [44]. We note that ℓ is much smaller than the zero temperature coherence length of 6.5 nm. We feel that the small value of ℓ is mainly attributed to the disorder, which is present in all alkali metal intercalated fulleride samples, including the best available single crystals. In this situation, i.e., $\ell << \xi_0$, fullerides are considered to be in the dirty limit. However, a low value of ℓ of about 1.0 nm is earlier reported by Ramirez and coworkers [67]. We further deduce the effective coherence length following $\xi_{00}^{-1} = \xi_0^{-1} + \ell^{-1}$ which leads to a value of about 0.88 nm. Henceforth, it is convenient to comment that the alkali metal intercalated fullerides are dirty superconductors defined by $\ell \le \xi_0, \xi_{00}$.

Furthermore, the magnetic penetration depth at T = 0 K as $\lambda_{L0}[=\sqrt{(m^* c^2/4\pi n e^2)}]$ estimated as 160 nm is slightly smaller than the values of 168 nm in Rb_3C_{60} [68]. The consistency is attributed to the proper choice of transport parameters as effective mass of carriers and carrier density as described in the beginning of 'Results and discussion' section. We now study the penetration depth dependence with temperature following $\lambda_L(T) = \lambda_L(0)[1 - (T/T_c)^4]^{-1/2}$. The variation of λ_L is shown in Figure 6 and notice that the curve manifests a power law consistent with the BCS behavior of penetration depth in conventional superconductors. As a next step, we determine the effective penetration depth following $\lambda_{L00} = \lambda_{L_0}\sqrt{\left[1+\xi_{00}\ell^{-1}\right]}$, yielding λ_{L00} of about 208.0 nm, consistent with the earlier estimate of 210 [69], 247 + 10, 247–20 [34,35], 370 nm [19], 460 nm [20], and 800 nm [22,70]. Furthermore, the lower critical field H_{c1} at T = 0 K is related to the coherence length ξ_0, and the London penetration depth λ_{L0} by the relation $H_{c1}(0) = \Phi_0 [4\pi\lambda_{L0}^2]^{-1}\ln[\lambda_{L0}/\xi_0]$, where Φ_0 is the magnetic flux quantum. Deduced

value of H_{c1} (0) is 25.8 mT that is comparable with the experimental value of 12 mT [34,35], 19 mT [69] and 26 mT [68]. Given the numbers that emerge from the analysis, it seems fair to conclude that AMIF is a conventional *s*-wave superconductor.

The other thermodynamical parameter as upper critical magnetic field is of importance as it denotes the magnetic field above which full magnetic flux penetration takes place and a transition from the superconducting to the normal state occurs. The upper critical field in the limit $T \to 0$ K is intimately related to coherence length as $H_{c2}(0) = \frac{\Phi_0}{2\pi\xi_0^2}$ and is obtained as 40 T. Magnetization measurements reveal a value of about 34 T [68], 55 T [71], 76 T [44], and 78 T [34,35]. Figure 7 shows the variation of upper critical field with temperature and manifests a power law following empirical relation: $H_{c2}(T) = H_{c2}(0)[1 - (T/T_c)^4]$.

The average value of critical magnetic field H_c (0) is found from the relation $H_c^2(0) = H_{c1}(0)\ H_{c2}\ (0)/\ln\ \kappa_0$ (κ_0 is the effective Ginzburg-Landau parameter) which is obtained as H_c (0) = 0.50 T which is consistent with the published data $H_c(0)$ (=0.44 T) [34,35]. The estimated value of $\kappa_0 = 56$ is much lower than the reported value of 84 [68], 90 [69], and 124 [34,35]. Furthermore, the slope of the upper critical field dH_{c2}/dT is estimated as −1.71 *T*/K, which is higher than the independent determination of about −3.8 *T*/K [44]. All the details regarding the thermodynamical variables describing the superconducting state for alkali metal intercalated fullerides are documented and listed in Table 1 along with the reported data. A more careful calculation with the choice of transport parameters presented in turn the deduced thermodynamical parameters which infer that AMIF superconductors belong to strongly type II superconductor and in a dirty limit.

We now discuss the method of calculation for pressure and volume effect on superconducting transition temperature in the test material. In order to analyze the pressure dependence of T_c for Rb_3C_{60} system, we

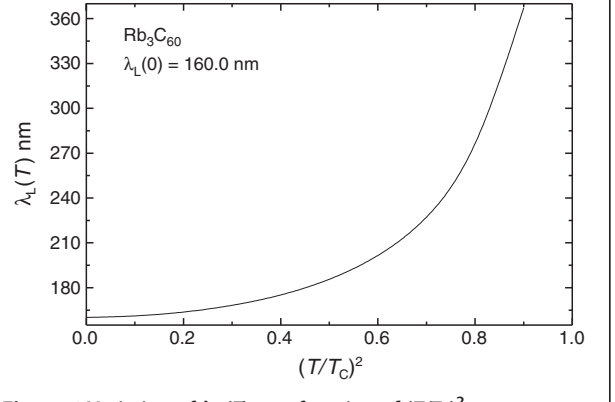

Figure 6 Variation of λ_L (*T*) as a function of $(T/T_C)^2$.

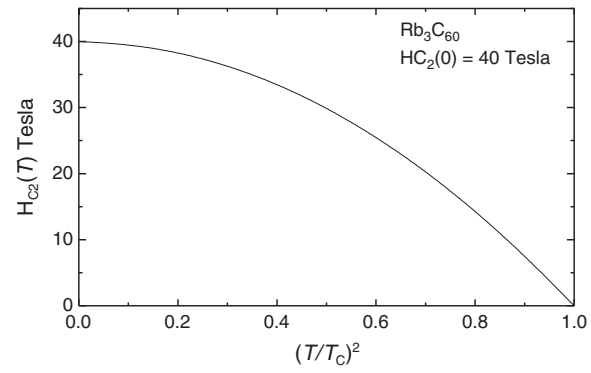

Figure 7 Variation of H_{c2} (*T*) as a function of $(T/T_C)^2$.

begin with the earlier developed Equation (25) according to which,

$$\frac{d\ln T_c}{dP} = \left[1 - \frac{\lambda_{ra}}{\lambda_{er}+\lambda_{ra}}\right]\frac{d\ln T_c^{er}}{dP} + \left[\ln\omega_{ra} - \ln T_c^{er}\right]\frac{d}{dP}\left[\frac{\lambda_{ra}}{\lambda_{er}+\lambda_{ra}}\right] + \left[\frac{\lambda_{ra}}{\lambda_{er}+\lambda_{ra}}\right]\frac{d\ln\omega_{ra}}{dP}. \quad (31)$$

Keeping in mind that C_{60} molecules are extremely rigid; hence, pressure neglecting the pressure-induced effects of intra-molecular phonons,

$$\frac{d\ln\omega_{ra}}{dP} = \frac{d\omega_{ra}}{dP} = 0. \quad (32)$$

Henceforth, we rewrite Equation (31) as

$$\frac{d\ln Tc}{dP} = \left[1 - \frac{\lambda_{ra}}{\lambda_{ra}+\lambda_{er}}\right]\frac{d\ln T_c^{er}}{dP} + \frac{1}{(\lambda_{er}+\lambda_{ra})^2}\left[\ln\left(\frac{\omega_{ra}}{T_c^{er}}\right)\right]\left[\lambda_{er}\frac{\lambda_{ra}}{dP} - \lambda_{ra}\frac{d\lambda_{er}}{dP}\right] \quad (33)$$

Furthermore,

$$\frac{d\ln T_c^{er}}{dP} = \frac{\partial\ln T_c^{er}}{\partial\lambda}\frac{d\lambda_{er}}{dP} + \frac{\partial\ln T_c^{er}}{\partial\omega_{er}}\frac{d\omega_{er}}{dP} + \frac{\partial\ln T_c^{er}}{\partial\mu^*}\frac{d\mu^*}{dP} \quad (34)$$

Using Equation (22), we get the following results:

$$\frac{\partial\ln T_c^{er}}{\partial\lambda}\frac{d\lambda_{er}}{dP} = D_{11}\frac{d\ln\lambda_{er}}{dP} \quad (35)$$

where

Table 1 Estimated physical parameters of Rb_3C_{60} along with the reported data

Sample number	Quantity	Symbol	Unit	Rb_3C_{60}	Reference
1	Lattice parameter of C_{60}	A	Å	14.20	[1-3]
2	Lattice parameter of K_3 C_{60}	A	Å	14.45	[1-3]
3	Bulk modulus	B	GPa	18.0	[59,60]
4	Force constant	κ	N/m	19.17	-
5	Force constant	κ'	N/m	1 κ	-
6	Mass of C_{60}	m	*amu*	1,431	-
7	Longitudinal phonon frequency	ω_L	10^{13} sec^{-1}	0.8	-
8	K-C distance	r_{mc}	Å	6.5	-
9	n-n distance	r_{cc}	Å	10.04	-
10	Mass of alkali atoms	M	*amu.*	366.92	-
11	Parameter	D_1	10^{13} sec^{-1}	0.52	-
12	Parameter	D_2	10^{13} sec^{-1}	0.38	-
13	Inter-molecular phonon frequency	ω_{er}	cm^{-1}	66.02	-
14	Charge carrier density	n_c	10^{21} cm^{-3}	4.0	-
15	Fermi wave vector	k_F	10^7 cm^{-1}	4.9	-
16	Effective mass	m^*	m_e	3.6	[58,73,74]
17	Fermi velocity	v_F	10^7 cm sec^{-1}	1.6	[49,50]
18	Fermi energy	ε_F	eV	0.25	0.2 to approximately 0.3 [4,5,38,63,64]
19	Plasma frequency	ω_p	eV	1.2	1.1 [70]
20	Density of states	$N(0)$	States/eV/spin	8.1	-
21	Screening length	κ_s^{-1}	Å	0.99	-
22	Dielectric function	ε_∞		4.4	[61]
23	Coulomb repulsive parameter	μ		0.90	-
24	E-P coupling strength	λ_{er}		1.17	-
25	Modified Coulomb parameter	μ^*		0.21	-
26	Effective coupling strength	λ_{eff}		0.57	-
27	Numerical function	$t(\lambda_{er})$		1.08	-
28	Transition temperature	T_c^{er}	K	4.17	-
29	Scattering rate	τ	10^{-14} s	0.8	0.7 ± 0.3 [73,74]
30	Intra-molecular phonon coupling strength	λ_{ra}		0.7	0.7
31	Normalized coupling parameter	^		0.37	-
32	Transition temperature	T_c	K	34.0	29.6 [1-3,34,35]
33	Coupling ratio	$\sigma(=\lambda_{er}/\lambda_{ra})$		1.67	-
34	Isotope exponent	α		0.30	0.37 ± 0.05 [10], 0.21 ± 0.012 [11]
				−0.092	−0.028 ± 0.06 [12], 0.21 [63,64], 0.32 ± 0.05 [67], −0.028 ± 0.06 [12]
35	Energy gap parameter	β		3.63	2.98 [17], 3.0 [18], 3.1 [20,21], 3.6 [19], 4.1 [24], 4.2 ± 0.2 [23], 5.2 ± 0.3 [16], 5.3 [25]
36	London penetration depth	λ_{L0}	nm	160	168 [68]
37	Coherence length	ξ_0	nm	2.86	2.0 [34,35,44], 3.0 [66]
38	Mean free path	ℓ	nm	1.28	0.9 [44], 1.0 [67]
39	Effective penetration depth	λ_{L00}	nm	208	210 [69], 247 + 10, 247 to 20 [34,35], 370 [19], 460 [20], 800 [22,70]
40	Effective coherence length	ξ_{00}	nm	0.88	-
41	Ginzburg-Landau parameter	κ_0		56	84 [68], 90 [69], 124 [34,35]

Table 1 Estimated physical parameters of Rb_3C_{60} along with the reported data *(Continued)*

42	Lower critical field	$H_{c1}(0)$	mTesla	25.88	12 [34,35], 19 [69], 26 [68]
43	Upper critical field	$H_{c2}(0)$	Tesla	40	34 [68], 55 [71], 76 [44], 78 [34,35]
44	Critical field	$H_c(0)$	Tesla	0.50	0.44 [34,35]
45	Temperature derivative of H_{c2}	dH_{c2}/dT	Tesla/k	−1.71	−3.8 [44]
46	Pressure constant	D_{11}	-	1.95	-
47	Pressure constant	D_{22}	-	−1.13	-
48	Pressure derivative of plasma frequency	$d\ln\omega_p/dP$	$\%GPa^{-1}$	2.77	-
49	Pressure derivative of density of states at Fermi level	$d\ln N(o)/dP$	$\%GPa^{-1}$	−3.70	−14.5 [36]
50	Pressure derivative of inter-molecular phonon frequency	$d\ln\omega_{er}/dP$	$\%GPa^{-1}$	11.11	-
51	Gruneisen parameter	γ_G		2.0	2.0 [36]
52	Pressure derivative of coupling strength	$d\ln\lambda_{er}/dP$	$\%GPa^{-1}$	−25.92	-
53	Pressure derivative of Coulomb repulsion	$d\ln\mu^*/dP$	$\%GPa^{-1}$	−0.47	-
54	Logarithmic pressure derivative of T_c	$d\ln T_c/dP$	$\%GPa^{-1}$	−29.41	−31.0 [36]
55	Slope	dT_c/dP	K GPa^{-1}	−9.9	−9.7 [34,35,37]
56	Volume derivative of coupling strength	$d\ln\lambda_{er}/d\ln V$		2.74	3.7 [72]
57	Residual resistivity	ρ_0	m Ω cm	0.22	0.22 [73,74]
58	Product	$k_F\ell$		6.27	-
59	Product	$\varepsilon_F\tau$		3.04	-

$$D_{11}=\frac{\lambda_{er}\left(\begin{array}{l}1+2\mu^*+0.28\lambda_{er}^2\mu^* t(\lambda_{er})\\ -0.28\lambda_{er}\mu^{*2}t(\lambda_{er})+\mu^{*2}t(\lambda_{er})\end{array}\right)}{(\lambda_{er}-\mu^*)^2}\times\left[1+\left\{\exp\left(\frac{2+4\mu^*+2\lambda_{er}\mu^* t(\lambda_{er})}{\lambda_{er}-\mu^*}\right)\right\}^{-1}+\left\{\exp\left(\frac{2+4\mu^*+2\lambda_{er}\mu^* t(\lambda_{er})}{\lambda_{er}-\mu^*}\right)\right\}^{-2}\right] \quad (36)$$

We use the following

$$\frac{\partial\ln T_c^{er}}{\partial\omega_{er}}\frac{d\omega_{er}}{dP}=\frac{d\ln\omega_{er}}{dP} \quad (37)$$

and

$$\frac{\partial\ln T_c^{er}}{\partial\mu^*}\frac{d\mu^*}{dP}=D_{12}\frac{d\ln\mu^*}{dP}, \quad (38)$$

$$D_{12}=-\frac{\mu*\left(1+2\lambda_{er}+\lambda_{er}^2 t(\lambda_{er})\right)}{(\lambda_{er}-\mu^*)^2}\left[1+\left\{\exp\left(\frac{2+4\mu^*+2\lambda_{er}\mu^* t(\lambda_{er})}{\lambda_{er}-\mu^*}\right)\right\}^{-1}+\left\{\exp\left(\frac{2+4\mu^*+2\lambda_{er}\mu^* t(\lambda_{er})}{\lambda_{er}-\mu^*}\right)\right\}^{-2}\right] \quad (39)$$

Combining these, we write

$$\frac{d\ln T_c^{er}}{dP}=D_{11}\frac{d\ln\lambda_{er}}{dP}+\frac{d\ln\omega_{er}}{dP}+D_{12}\frac{d\ln\mu^*}{dP} \quad (40)$$

Herein, the first and the third terms are dependent on the variation of the $N(0)$ with pressure.

In order to make progress, we have used the value B = 18 GPa and ε_F = 0.25 eV as documented in the previous section. The free electron gas result $d\ln N(0)/dP = (-2/3)\,\kappa_T$, where κ_T (approximately B^{-1}), is the thermal compressibility. The calculated value of $d\ln N\,(0)/dP$ is about −3.70% $(GPa)^{-1}$. However, Diederich and coworkers reported a rate of about −14.5% $(GPa)^{-1}$ [36] although of limited accuracy. From Equations (11) and (13), we write

$$\frac{d\ln\mu^*}{dP}=\frac{d\ln N(0)}{dP}\left(\frac{\mu^*}{\mu}\right)-\mu^*\left[\frac{2d\ln\omega_p}{dP}-\frac{d\ln N(0)}{dP}-\frac{d\ln\omega_{er}}{dP}\right] \quad (41)$$

$$\frac{d\ln\lambda_{er}}{dP}=\frac{d\ln N(0)}{dp}-\frac{d\ln\langle\omega_{er}^2\rangle}{dP}, \quad (42)$$

where the pressure dependence of the quantity $<I^2>$ has been neglected. Using Equations (41) and (42) into Equation (40), we obtain:

$$\frac{d\ln T_c^{er}}{dP}=\left[D_{11}+D_{12}\left(\frac{\mu^*}{\mu}\right)+D_{12}\mu^*\right]\frac{d\ln N(0)}{dP}+[1-2D_{11}+D_{12}\mu^*]\frac{d\ln\omega_{er}}{dP}-2D_{12}\mu^*\frac{d\ln\omega_p}{dP} \quad (43)$$

Here, we assume: $d\ln\lambda_{ra}/dP \approx d\ln N\,(\varepsilon_F)/dP$, $d\ln<\omega_{er}^2>/dP \approx 2d\ln<\omega_{er}>/dP$ and $d\ln<\omega_{er}>/dP \approx d\ln\omega_{er}/dP$. The

free electron estimate for $dln\omega_p/dP = 1/2B$ yields a value of about 2.77% $(GPa)^{-1}$. We follow $\gamma_G = B\ d\ln<\omega>/dP$ to obtain $d\ln\omega_{er}/dP = 11.11\%\ (GPa)^{-1}$, using $\gamma_G = +2$ as earlier reported [37]. The parameters needed for further calculations are obtained as $D_{11} = 1.95$ and $D_{12} = -1.13$ from the values of $\lambda_{er} = 1.17$, $\mu = 0.90$, and $\mu^* = 0.21$. Using Equations (33) to (43), we find the value of $d\ln\mu^*/dP = -0.47\%\ (GPa)^{-1}$, $d\ln\lambda_{er}/dP = -25.92\%\ (GPa)^{-1}$, $d\ln\lambda_{ra}/dP = -3.70\%\ (GPa)^{-1}$, $d\ln T_c^{er}/dP$ is $-38.89\%\ (GPa)^{-1}$, $d\ln T_c/dP = -29.41\%\ (GPa)^{-1}$is well consistent with the experimental data $d\ln T_c/dP = -31.0\%/(GPa)$ [36] and slope $dT_c/dP = -9.9$ K/GPa which is well consistent with the earlier reported value [34,35,37] of −9.7 K/GPa. Figure 8 shows the variation of T_c with pressure along with the experimental data. For fitting of the data, we have employed the relation $T_c\ (P) = T_c\ (0)\ \exp\ [-0.2\gamma P]$ using $\gamma_G = +\ 2$ [36]. We follow the discussion and results of Sparn and coworkers who fit the data using $T_c\ (P) = T_c\ (0)\ \exp\ [-\gamma P]$ with $\gamma = 0.44 \pm 0.03\ GPa^{-1}$ [34,35]. We therefore reach the conclusion that the logarithmic derivative of the Coulomb pseudopotential with pressure, $d\ln\mu^*/dP$, is smaller as compared to the other logarithmic derivatives involved in the expression of superconducting transition temperature as we dealt with.

We appeal from the model calculations that the pressure dependence of T_c in fullerides shows its metallic characteristic. In principle, the electron–phonon coupling parameter is directly proportional to the density of states at the Fermi level and inversely proportional to appropriately averaged square of the inter-molecular optical phonon frequency. The variation of T_c with pressure is thus dependent on the variation of the density of states at Fermi level, the Coulomb pseudopotential, and the variation of the characteristic phonon frequency with pressure. We end by stating that both T_c and its pressure dependence in Rb_3C_{60} are dictated by the properties of both inter- and intra-molecular vibrations. To test this idea, it will also be interesting to investigate the volume derivative of T_c.

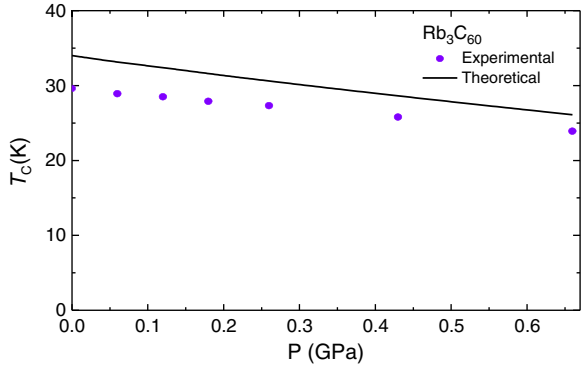

Figure 8 Variation of T_c with pressure. Closed circles represent the experimental data taken from Sparn et. al. [34,35].

We now explore our efforts in studying the volume derivative of T_c or dT_c/dV. Such studies point to either weak or strong coupling of mediating bosons. We note that due to extreme rigidity of C_{60} the compression contracts the weak inter-molecular bonds and high-energy intra-molecular bonds are unaffected. With these considerations, Equation (25) simplifies to the following relation,

$$\frac{dT_c}{dV} = T_c^{er}\frac{d}{dV}\left[\frac{\omega_{ra}}{T_c^{er}}\right]^{\Lambda} + \left[\frac{\omega_{ra}}{T_c^{er}}\right]^{\Lambda}\frac{dT_c^{er}}{dV} \tag{44}$$

which leads to the following result

$$\frac{dT_c}{dV} = (1-\Lambda)\left[\frac{\omega_{ra}}{T_c^{er}}\right]^{\Lambda}\frac{dT_c^{er}}{dV} \tag{45}$$

With an assumption that intra-molecular phonons are independent in any change of the volume [69],

$$\frac{d\ln\omega_{ra}}{dV} = \frac{d\omega_{ra}}{dV} = 0 \tag{46}$$

Following Equation (22), we write

$$\frac{dT_c^{er}}{dV} = \frac{0.25}{\left[\exp\left(2/\lambda_{eff}\right)-1\right]^{1/2}}\times\frac{d\omega_{er}}{dV} + \frac{\exp\left(2/\lambda_{eff}\right)}{\left[\exp\left(2/\lambda_{eff}\right)-1\right]^{3/2}}\times\left(\frac{0.25\omega_{er}}{\lambda_{eff}^2}\right)\frac{d\lambda_{eff}}{dV} \tag{47}$$

where,

$$\frac{d\lambda_{eff}}{dV} = \left\{\frac{1+2\mu^*+\mu^{*2}t(\lambda_{er}) - 0.28\lambda_{er}\mu^{*2}t(\lambda_{er}) + 0.28\lambda_{er}^2\mu^* t(\lambda_{er})}{(1+2\mu^*+\lambda_{er}\mu^* t(\lambda_{er}))^2}\right\}\frac{d\lambda_{er}}{dV} - \left\{\frac{1+2\lambda_{er}+\lambda_{er}^2.t(\lambda_{er})}{(1+2\mu^*+\lambda_{er}\mu^* t(\lambda_{er}))^2}\right\}\frac{d\mu^*}{dV} \tag{48}$$

Using Equations (49) and (47), we write

$$\frac{dT_c}{dV} = D_{21}\frac{d\omega_{er}}{dV} + D_{22}\frac{d\lambda_{er}}{dV} - D_{24}\frac{d\mu^*}{dV} \tag{49}$$

Here, we define

$$D_{21} = V_{00}\left\{\frac{0.25}{\left(\exp\left(2/\lambda_{eff}\right)-1\right)^{1/2}}\right\}, \tag{50}$$

$$D_{22} = V_{00}\left\{\frac{\exp(2/\lambda_{eff})}{(\exp(2/\lambda_{eff})-1)^{3/2}} \times \frac{0.25\omega_{er}}{\lambda_{eff}^2}\right\} \left\{\frac{1+2\mu^*+\mu^{*2}t(\lambda_{er}) - 0.28\lambda_{er}\mu^{*2}t(\lambda_{er}) + 0.28\lambda_{er}^2\mu^* t(\lambda_{er})}{(1+2\mu^*+\lambda_{er}\mu^* t(\lambda_{er}))^2}\right\}, \quad (51)$$

and

$$D_{23} = V_{00}\left\{\frac{\exp(2/\lambda_{eff})}{(\exp(2/\lambda_{eff})-1)^{3/2}} \times \frac{0.25\omega_{er}}{\lambda_{eff}^2}\right\} \left\{\frac{1+2\lambda_{er}+\lambda_{er}^2 t(\lambda_{er})}{(1+2\mu^*+\lambda_{er}\mu^* t(\lambda_{er}))^2}\right\} \quad (52)$$

where

$$V_{00} = \left(\omega_{ra}/T_c^{er}\right)^{\frac{\lambda_{ra}}{\lambda_{er}+\lambda_{ra}}}\left(1-\frac{\lambda_{ra}}{\lambda_{er}+\lambda_{ra}}\right) \quad (53)$$

Furthermore, the logarithmic volume derivative of the coupling parameter λ follows:

$$\frac{d\ln\lambda}{d\ln V} = B\frac{d\ln N(0)}{dP} + 2\gamma_G \quad (54)$$

leads to the ratio

$$\Phi = \frac{d\ln\lambda}{d\ln V} \quad (55)$$

with the values of B, $d\ln N(\varepsilon_F)/dP$ and $d\ln<\omega>/dP$ discussed earlier, we find $\Phi = 5.3$ for Rb_3C_{60}. In passing, we note that the value of Φ for AMIF is comparable to the value of $\Phi = 3.7$ for usual metals as aluminum [72].

To ascertain the physical significance of the volume derivative of T_c, we estimate the parameters as $D_{21} = 0.23$, $D_{22} = 36.94$, and $D_{23} = -115.56$ from the earlier mentioned values of various coupling strengths. Looking at Equation (49), dT_c/dV is being influenced by (a) volume dependence of screening parameter, (b) volume dependence of inter-molecular vibrational mode, (c) volume dependence of inter-molecular phonon coupling strength, and (d) the intra-molecular phonon frequency as well as the various coupling parameters independent of volume. Because of the difficulties in determining the volume derivative of molecular phonon frequency, we are only able to provide some suggestive formal argument below.

Generally, the compression increases the bandwidth; hence, the ε_F resulted in the reduction of renormalized screening parameter. We note that the Coulomb repulsion suppresses T_c as is being noticed from Figure 1. Henceforth, the contribution to dT_c/dV proportional to $d\mu^*/dV$ is negative. We follow Crespi and Cohen [73,74] who argue that the logarithmic dependence of μ^* on ε_F points to the fact that volume derivative of μ^* is small in magnitude. A natural argument follows that the volume derivative of $t(\lambda)$ and of μ^* is small compared to $d\lambda/dV$; henceforth, we neglect these two terms in Equation (49). In summary, inter-molecular phonon frequencies are influenced under compression modes and if superconductivity in the fullerenes arises from coupling to inter-molecular phonons, then this argument implies strong electron–phonon coupling. Thus, we expect that the volume derivative of transition temperature is positive and large in AMIF.

We now discuss and compute numerically the response of resistivity in Rb_3C_{60}. In usual metals, the electron–phonon scattering is a major source of temperature-dependent resistivity and can describe the normal state transport properties. However, apart from electron–phonon scattering, other scattering mechanisms as electrons scatter off impurities, defects, grain boundaries, and disordered regions lead to a temperature-independent contribution. Let us begin with the estimation of the temperature-independent contribution to resistivity.

Information of zero temperature elastic scattering rate and plasma frequency will allow us to have an independent estimation of zero temperature-limited resistivity. The zero temperature scattering rates are related through the upper critical magnetic field H_{c2} (0). Following the two-square-well analysis of Eliashberg theory, Carbotte suggested that the strong coupling corrections are important and a rescaling factor of 1+ λ appears in the modified BCS results [75]. The Matsubara gap function, which is related with upper critical magnetic field, yields

$$\frac{1+\lambda}{\lambda-\mu^*} = 2\pi\frac{T}{T_c}\sum_{m=0}^{N_c}\frac{1}{\chi_m^{-1}(\bar{\omega}m)-(2\tau)^{-1}} \quad (56)$$

$\bar{\omega}m$ being the Matsubara frequency, within the standard two-square-well model and is $\bar{\omega}m = \omega_m(1+\lambda) + (2\tau)^{-1}(\text{sgn}\,\omega_m)$, λ is the electron–phonon coupling strength with cut off at N_c, and τ the scattering time. In this approximation, N_c follows [75]

$$N_c = \frac{1}{2}\left[\frac{\omega}{\pi T}+1\right] \quad (57)$$

μ^* is the renormalized Coulomb repulsive parameter and the factor χ_m appearing in Equation (56) is

$$\chi_m(\bar{\omega}m) = \frac{2}{\sqrt{\xi^*}}\int_0^\infty \exp(-q^2)\tan^{-1}(\phi)dq, \quad (58)$$

with

$$\phi = \frac{q\sqrt{\xi^*}}{\left[(2m+1)\pi\frac{T}{T_c}\right] + \left[\frac{1}{2\tau^*}\right]}. \tag{59}$$

The upper critical magnetic field is related through

$$\xi^* = \frac{1}{2}eH^*_{c2}v^{*2}_F \tag{60}$$

The physical quantities appearing in equations (56–60) involve renormalized values as

$$H^*_{c2} = \frac{H_{c2}}{(1+\lambda)T_c}, \tag{61}$$

$$v^*_F = \frac{v_F}{\sqrt{(1+\lambda)T_c}}, \tag{62}$$

and impurity scattering time

$$\tau^* = \frac{\tau}{(1+\lambda)T_c} \tag{63}$$

These equations differ from the BCS limit, as the renormalizations in ξ^*, v_F^*, H^*_{c2}, and τ^* are introduced. These expressions are valid for any impurity concentration described in Equations (56) to (60) by scattering time. In the present analysis, Pauli limiting has been neglected as an approximation due to relatively small value of dH_{c2}/dT $[1/(1+\lambda)]$ in alkali metal intercalated fullerenes [76]. In principle, the above approach describes quantitatively the renormalization of the physical properties due to the electron–phonon interaction and is therefore reduced by $1+\lambda$.

The zero temperature-limited resistivity is expressed as

$$\rho(0) = \frac{4\pi\tau^{*-1}}{\omega_p^2} \tag{64}$$

From the above, it is noticed that the determination of scattering rate essentially needs the Coulomb repulsive parameter, electron phonon coupling strength, Fermi velocity, plasma frequency, and the upper critical magnetic field. This allows one to estimate the zero temperature-limited resistivity independently.

We use the earlier deduced value of H_{c2} (0) = 40 Tesla, $T_c = 34\,K$, $v_F = 1.6 \times 10^7$ cm sec^{-1}, and $\omega_p = 1.2$ eV to estimate the zero temperature elastic scattering rates which is obtained as 0.8×10^{-14} s and is consistent to the experimental value τ (= $0.7 \pm 0.3 \times 10^{-14}$ s) as those derived from the superconducting fluctuation measurements [41,73,74]. It is attributed to the fact that the larger the electron mass, the smaller the plasma frequency and hence reduced zero temperature elastic scattering rate. We have earlier estimated the zero temperature mean free path, ℓ of about 1.28 nm which is highly sensitive for carrier scattering. We further find that the product $k_F\ell$ (approximately 6.27) seems to be much larger than the unity which indicates the metallic characteristics. It is worth to mention that the product $\varepsilon_F\tau >> 1$ in the test material refers to the fact that the doped fullerides fall in the weak scattering limit. This is however, consistent with the *s*-wave superconductors. With these parameters, we estimate that the zero temperature-limited resistivity ($\rho_0 = 0.22$ m Ω cm) is consistent with the reported value [73,74] and is used later to estimate the electron–phonon resistivity.

We complete our model calculations by looking at the temperature-dependent resistivity for Rb_3C_{60} superconductors. To formulate a specific model, we start with the general expression for the temperature-dependent part of the resistivity [77] given by

$$\rho = \frac{3\pi}{\hbar e^2 v_F^2}\int_0^{2k_f} |v(q)|^2 |S(q)|^2 \left(\frac{1}{2k_F}\right)^4 q^3 dq, \tag{65}$$

where v (q) is the Fourier transform of the potential associated with one lattice site, and $S(q)$ the structure factor, and following the Debye model, it takes the following form

$$|S(q)|^2 \approx \frac{k_B T}{M v_s^2} f(\hbar\omega/k_B T) \tag{66}$$

$$f(x) = x^2[e^x - 1]^{-1}[1 - e^{-x}]^{-1} \tag{67}$$

f(x) represents the statistical factor.

Thus, the resistivity expression leads to

$$\rho \approx \left(\frac{3}{\hbar e^2 v_F^2}\right)\frac{k_B T}{M v_s^2}\int_0^{2k_F} |v(q)|^2 \left[\frac{(\hbar\omega/k_B T)^2 q^3 dq}{(\exp(\hbar\omega/k_B T) - 1)(1 - \exp(-\hbar\omega/k_B T))}\right], \tag{68}$$

where v_s is the sound velocity. Equation (68) in terms of inter-molecular phonon contribution yields the Bloch-Gruneisen function of temperature-dependent resistivity:

$$\rho_{er}(T, \theta_{er}) = 4A_{er}(T/\theta_{er})^4 \times T\int_0^{\theta_{er}/T} x^5 (e^x - 1)^{-1}(1 - e^{-x})^{-1} dx, \tag{69}$$

where $x = \hbar\omega/k_B T$, while A_{er} is the constant of proportionality defined as

$$A_{er} \cong \frac{3\pi^2 e^2 k_B}{k_F^2 v_s^2 L \hbar v_F^2 M} \tag{70}$$

In view of inelastic neutron scattering measurements, the phonon spectrum can be conveniently separated into

two parts of phonon density of states [6,7]. Therefore, it is natural to choose a model phonon spectrum consisting of two parts: an inter-molecular phonon frequency ω_{er} (θ_{er}) and an intra-molecular phonon frequency ω_{ra} (θ_{ra}). If the Matthiessen rule is obeyed, the resistivity may be represented as a sum $\rho(T) = \rho_0 + \rho_{e\text{-}ph}$ (T), where ρ_0 is the residual resistivity that does not depend on temperature as described earlier. On the other hand, in case of the intra-molecular phonon spectrum, ρ_{ra} (T) may be described as follows

$$\rho_{ra}(T,\theta_{ra}) = A_{ra}\theta_{ra}^2 T^{-1}[\exp(\theta_{ra}/T) - 1]^{-1} \times [1 - \exp(-\theta_{ra}/T)]^{-1}, \quad (71)$$

where A_{ra} is defined analogously to Equation (70). Finally, the phonon resistivity can be conveniently modeled as

$$\rho_{e-ph}(T) = \rho_{er}(T,\theta_{er}) + \rho_{ra}(T,\theta_{ra}). \quad (72)$$

Henceforth, the total resistivity is now rewritten as

$$\begin{aligned}\rho(T,\theta_{er},\theta_{ra}) &= \rho_0 + \rho_{er}(T,\theta_{er}) + \rho_{ra}(T,\theta_{ra}) \\ &= \rho_0 + 4A_{er}(T/\theta_{er})^4 T \\ &\quad \times \int_0^{\theta er/T} x^5(e^x - 1)^{-1}(1 - e^{-x})^{-1}dx \\ &\quad + A_{ra}\theta_{ra}^2 T^{-1}[\exp(\theta_{ra}/T) - 1]^{-1} \\ &\quad [1 - \exp(-\theta_{ra}/T)]^{-1}. \end{aligned} \quad (73)$$

Though this is a purely phenomenological expression, it seems to provide a reasonable description of the available experimental data. Now, we proceed to evaluate the temperature-dependent contribution in Rb_3C_{60} superconductor.

Figure 9 illustrates the results of temperature dependence of resistivity via the ordinary electron–phonon interaction from Equation (73) with our choice of inter-molecular phonon frequency ω_{er} (=95 K) and intra-molecular phonon frequency ω_{ra} (=1,220 K). The contributions of inter-molecular and intra-molecular phonon towards resistivity are shown separately along with the total resistivity. It is inferred from the curve that ρ_{er} increases linearly, while ρ_{ra} increases exponentially with the increase in temperature. Both the contributions are clubbed together, and the resultant resistivity is exponential at low temperatures and nearly linear at high temperatures until room temperature.

Our numerical results on temperature dependence of resistivity of Rb_3C_{60} are plotted in Figure 10 along with the single crystal data [41]. It is noticed from the plot that the estimated ρ is lower than the reported data from T_c to near room temperature. Deduced values of the temperature-dependent ρ from Equation (73) appear low, as ρ_0 and ω_p values are the constraints for the present analysis. Thus, estimated model parameters (λ, μ^*, ν_F, ω_p, τ, and $\rho(0)$) represent a good set of parameters for the estimation of normal state resistivity in alkali metal intercalated fullerides. Nevertheless, the role of electron–phonon interaction is better exploited and found prominent in the interpretation of normal state transport parameters.

The difference between the measured ρ and calculated $\rho_{diff.}$ [$=\rho_{exp.} - \{\rho_0 + \rho_{e-ph}$ ($=\rho_{er} + \rho_{ra}$)}] is plotted in Figure 11. A power temperature dependence of $\rho_{diff.}$ is inferred at low (approximately 22 to 200 K) temperature, and it becomes almost saturated at higher temperature. The quadratic temperature contribution at low temperature for resistivity is an indication of conventional electron–electron scattering. The feature of quadratic temperature dependence of $\rho_{diff.}$ is similar to that of electron-doped cuprate and bismuthate superconductors, which is an artifact of electron–electron scattering [78,79]. The departure from linear T^2 behavior of ρ_{diff} may be due to the dimensionality crossover

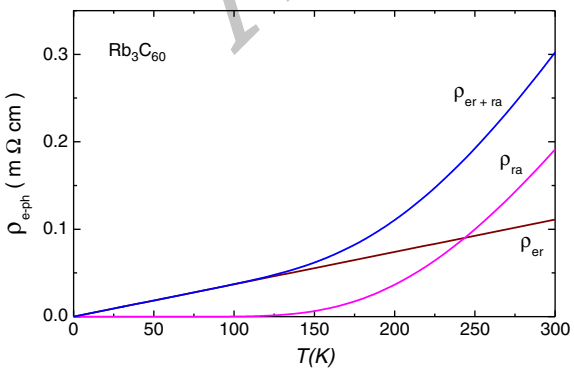

Figure 9 The results of temperature dependence of resistivity via the ordinary electron–phonon interaction from Equation (73). Variation of $\rho_{e\ -\ ph}$ with temperature. The contribution of ρ_{er} as well of ρ_{ra} to the resistivity.

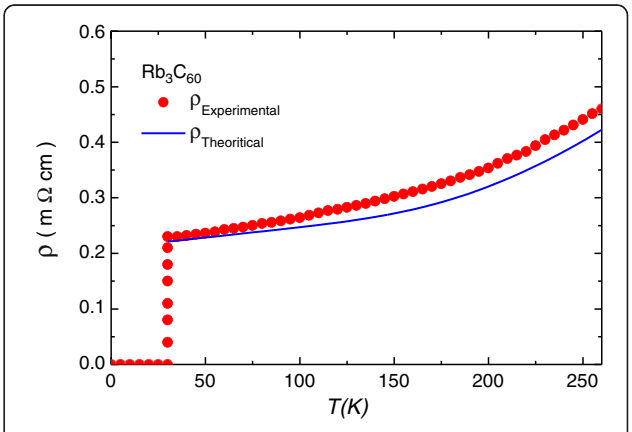

Figure 10 Variation of ρ with temperature T (K). Open circles represent the experimental data taken from [74].

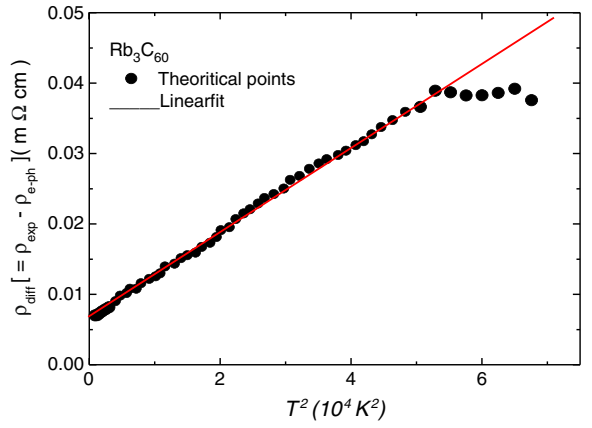

Figure 11 Variation of $\rho_{diff.}$ [$=\rho_{exp.} - \{\rho_0 + \rho_{e-ph}\ (=\rho_{er} + \rho_{ra})\}$] with T^2.

if any. The additional term due to electron–electron contribution was required to understand the resistivity behavior, as extensive attempts to fit the data with residual resistivity and phonon resistivity were unsuccessful. It is noteworthy to comment that in conventional metals, the electron–electron contribution to the resistivity can at best be seen at higher temperatures due to its small magnitude at low temperature when comparison is made with phonon contribution. We have thus demonstrated the role of electron–phonon scattering versus electron–electron interaction effects in determining the normal state resistivity of fullerides.

The existence of quadratic temperature dependence of resistivity over a wide temperature interval permits one to believe that the electron–electron scattering is also significant in determining the resistivity in alkali metal intercalated fullerides. It is worth to refer to an earlier work of Thompson [80], who postulated the power temperature dependence of electro-resistivity in TiS_2 as a consequence of low carrier concentration. Correlating this concept, alkali metal intercalated fullerenes have definitely low carrier concentration (approximately 10^{21} cm^{-3}) and may result in a large enhancement of power temperature dependence of electrical resistivity even up to room temperature.

In this manner, one can shed further light by correlating the magnitude of electron–electron contribution to resistivity with plasma frequency. If the quadratic temperature dependence of resistivity is a cause of three-dimensional electron–electron scattering (umklapp), then its magnitude should depend on the carrier concentration n as $n^{-5/3}$ or equivalently on the plasma frequency as $\omega_P^{-10/3}$. In this scenario, we estimate ρ_{ee} of about 0.6 m Ω cm (as illustrated in Figure 3) with $\omega_P^{-10/3}$ as 0.54 (eV) $^{-10/3}$ for ρ_0 value of 0.22 m Ω cm in the vicinity of room temperature. In conclusion, both qualitatively and quantitatively, our results strongly suggest that all the three scales as Coulomb, acoustic, and optical phonons are important in high-T_c cuprates.

In passing, we note that Crespi and coworkers have argued that electron–electron scattering mechanism is contributing to the normal state resistivity of Rb_3C_{60} superconductors [46]. Furthermore, they have used Ziman's formula in analyzing the single crystal Rb_3C_{60} resistivity data. While interpreting the data, they have used the value of coupling strength, i.e., λ_{high} and λ_{low}, as well as the molecular phonon frequencies from various theoretical models of the electron–phonon coupling, and using $\alpha^2 F(\omega)$ corresponding to a uniformly scaled version of the inelastic neutron scattering intensity. On the other hand, in the present model calculations, we have used the coupling strength for electron–phonon coupling as deduced from the density of states, electron–phonon interaction matrix, and the inter- and intra-molecular phonon frequency. The electron-ion matrix is derived from the Coulomb potential with static dielectric function in the long wavelength limit. Interestingly, the enhanced density of states adds the screening effect, which is properly incorporated in Coulomb potential.

Finally, we refer to a recent photoemission spectra analysis of Rb_3C_{60} that points to the metallicity of AMIF as a result of charge fluctuation that occurs due to competition between the electron–electron as well as electron–phonon interaction [81]. However, there are several reports which emphasize the importance of including both interactions in the understanding of fullerides [82]. Thus, one cannot escape stating that the temperature dependence of normal state resistivity in alkali metal doped fulleride is better understood by the three component model as $\rho = \rho_o + \rho_{e-ph} + \rho_{e-e}$. Moreover, considering the fulleride problem, one cannot rule out that all the energy scales ω_{er} (inter-molecular vibrations), ω_{ra} (inter-molecular vibrations), and ω_c (the Coulomb interactions) are essential for retrieving the documented behavior of normal state resistivity.

We comment that besides electrical resistivity in doped fullerides, the high T_c, the pressure effect, the coupling strengths, the retardation effects, and the competitive nature of electron-inter-molecular, electron-intra-molecular interactions, and Coulomb screening are significant in fulleride superconductors [83-91].

Conclusion

In this communication, we have devoted our efforts in revealing the attractive pairing mechanism and various physical parameters of alkali metal intercalated fullerene superconductor within the framework of strong coupling theory. The particular system chosen for the study, because huge experimental data is available, consistent explanation is timely needed. Considering the three-

dimensional Rb_3C_{60} as a diatomic lattice of Rb and C_{60}, we have derived expression for inter-molecular (acoustic and optical) phonon modes. Considering the importance of experimental constraints on high temperature superconducting theories, we have properly used the Bulk modulus as well as other structural parameters. The inter-molecular optical phonon frequency obtained and used frequency of intra-molecular phonon are in consonance with the recent theoretical and experimental findings. We have employed the superconducting state parameters, i.e., (a) the transition temperature (T_c), (b) the carbon isotope effect (α), (c) the energy gap parameter (β), (d) the pressure as well as volume effect on T_c, (e) the thermodynamical parameters describing the superconducting state, and (f) the electrical resistivity in alkali metal intercalated fulleride superconductors. We have presented our results on AMIF in terms of *s*-wave pairing state.

The appropriateness of the proposed approach depends on proper consideration of the structure for 8 N C_{60}-Rb bonds, out of which 4 N are at octahedral position and 4 N take the tetrahedral sites. Due to the simplicity of the approach, the estimated values of T_c, α, β, and $d\ T_c/dP$ are consistent with the reported data. The deduced value of coupling strength for the inter-molecular phonons (optical) favors the strong coupling mechanism. By finding that intra-molecular phonons do play a significant role, we have obtained a steep increase in T_c. Unlikely, the coupling strength for intra-molecular phonons is an indicative of weak coupling theory.

Although, in the present investigation, we have introduced the intra-molecular phonons in an *ad hoc* way and obtained an analytical result, we do not claim it to be a rigorous expression. However, it is illustrated that the intra-molecular phonon pairing mechanism must be a viable mechanism for alkali metal fullerides. Various reports strongly favor the intra-molecular vibrations as a key source of superconductivity and claim that inter-molecular phonons will not induce the state; still we believe and argue that both the inter- and intra-molecular phonons participate in the superconducting state as well as essential for superconducting fulleride properties as transition temperature, carbon isotope effect, energy gap parameter, and pressure effect. Our results are of interest and provide a test of the possibility of the cooperative mechanism in alkali metal fulleride superconductors.

To account for high T_c in doped fullerides, we have studied carefully the dependence of T_c on various coupling strength parameters and we found the condition $\mu^* < \mu,\ \lambda_{er}(\lambda_{ra}) - \mu^* > 0$ for high T_c superconductivity. We find that T_c strongly depends on the Coulomb repulsive parameter and is higher for small values of μ. Also, using the scaling factor as ω_{er} while estimating the screening parameter, we correctly represent the retardation effects that are small. As the Fermi energy is larger at least an order of magnitude by inter-molecular phonons, the retardation effects are expected to be very small. On the other hand, the Fermi energy and intra-molecular phonon frequency are almost of similar order; hence, vertex correction becomes important because the Migdal theorem does not hold and the frequency dependence of the effective Coulomb interaction must be considered in fullerides.

Although we have provided a simple phenomenological explanation of screening parameter in fullerides, there is clearly a need for a detailed theoretical understanding of vertex corrections and shall be covered in near future. Generally, energy ω_b is presented as characterizing bosons (ω_{er} or ω_{ra}), but opinion about its choice is far from being unanimous. Lastly, T_c increases steeply with the enhanced value of either λ_{er} or λ_{ra} value. It is fair to comment that this is not the first time a dominant signature of intra-molecular phonons for superconducting state is claimed.

A central prediction of the proposed approach is the evaluation of the carbon isotope effect exponent. The analysis predicts a reduced value of α when comparison is made with the BCS limit. Reduced α value strongly favors the strong coupling mechanism in Rb_3C_{60}. While considering the inter-molecular phonons using the obtained T_c^{er}, the energy gap appears higher, while when intra-molecular phonons are considered, the energy gap is comparable with the BCS result. We argue that the reduced value of α essentially points to the large Coulomb repulsion apart from large electron–phonon coupling strength. Deduced results on α and β are consistent with the earlier reported data. It is inferred that electron pairing with inter-molecular phonons would lead to a strong coupling, while with the intra-molecular phonons require weak coupling mechanism. Although several reports strongly favor the intra-molecular vibrations as a key source of superconductivity and claim that inter-molecular phonons will not induce the state, the present analysis reveals that both the inter- and intra-molecular phonons participate in the superconducting state.

In addition, the model calculations reveal that the coherence length which, even if small, is much larger than inverse Fermi momentum. The zero temperature mean free path, ℓ, is much smaller than the zero temperature coherence length. We hope that the small value of ℓ is mainly attributed to the disorder, which is present in all alkali metal intercalated fulleride samples, including the best available single crystals. In this situation, i.e., $\ell << \xi_0$, fullerides are considered to be in the dirty limit. Henceforth, it is convenient to comment that the alkali metal intercalated fullerides are dirty superconductors of type-II.

The appreciation of the model calculations with both Coulomb and molecular (inter and intra) phonons is

revealed from the fact that several experimental facts concerning the superconducting state in alkali metal intercalated fullerides turn out to be explained in this work. We have also discussed the pressure dependence of dT_c/dP. We expect from the model calculations that the pressure dependence of T_c demonstrates the metallic behavior. The appreciation reveals that the developed expression yields a value of dT_c/dP close to the reported data. In principle, the electron–phonon coupling parameter is directly proportional to the density of states at the Fermi level and inversely proportional to appropriately averaged square of the molecular phonon frequency. The variation of T_c with pressure is thus dependent on the variation of the Fermi level density of states, the Coulomb pseudopotential, and the variation of the phonon frequency with volume. The pressure effect in AMIF is huge; pressure derivative of T_c is negative, while the volume derivative of T_c is positive. We end by stating that both T_c and its pressure (volume) dependence in Rb_3C_{60} are dictated by the properties of inter- and intra-molecular vibrations.

Furthermore, we showed that the volume derivative of T_c is being influenced by (a) volume dependence of screening parameter, (b) volume dependence of inter-molecular vibrations, (c) volume dependence of intermolecular phonons, and (d) the intra-molecular phonon frequency, as well as the various coupling parameters independent of volume. Generally, the compression increases the bandwidth; hence, the ε_F resulted in the reduction of renormalized screening parameter. Usually, the Coulomb repulsion suppresses the T_c. Henceforth, the contribution to dT_c/dV proportional to $d\mu^*/dV$ is negative. In continuation, the volume derivative of $t(\lambda)$ and of μ^* is small compared to $d\lambda/dV$. We believe that inter-molecular phonon frequencies are influenced under compression modes and if superconductivity in the fullerenes arises from coupling to inter-molecular phonons, then this argument implies strong electron–phonon coupling. Mention may be made that in AMIF, the volume derivative of transition temperature is positive and large.

Within the framework of Bloch-Gruneisen theory, we find that the normal state resistivity of alkali metal-doped fullerenes is consistent with single crystal data for Rb_3C_{60} superconductors. Keeping in mind the importance of experimental constraints on theories, we have properly used the structural information like intra-molecular and inter-molecular phonon frequencies. We succeeded in explaining the normal state resistivity and other associated transport parameters by the electron–phonon interaction. We have first estimated the zero temperature elastic scattering rate with the use of the parameters (λ, μ^*, ν_F, τ, H_{c2} (0), and ω_p) from the developed approach. Furthermore, the zero temperature mean free path is found to be smaller than the zero temperature coherence length.

The larger mean free path and product $k_F L >> 1$ favor the metallic conduction. Hence, the use of Bloch-Gruneisen expression in estimating the electron–phonon contributions is appropriate. It is noticed that contribution from inter-molecular phonon and intra-molecular phonon together with the zero temperature-limited resistivity is smaller than the reported data on the single crystal. The temperature dependence of resistivity in doped fullerides can be conveniently described by the usual electron–phonon interaction. In view of inelastic neutron scattering data, the phonon spectrum is conveniently separated into two parts, inter-molecular and intra-molecular phonons. The high-energy intra-molecular phonon yields a large contribution to the resistivity. In turn, large value of electron–phonon coupling strength is no doubt from the intra-molecular phonons. We note that the product $\varepsilon_F \tau >> 1$ in the test material refers to the fact that the doped fullerides fall in the weak scattering limit.

When the subtracted data is plotted as a function of T^2, a clear straight line is depicted from 34 to 200 K, but it becomes saturated at further higher temperature. The observation of T^2 dependence points toward the electron–electron scattering and departure from T^2 behavior is an outcome of dimensionality crossover, if any, in these alkali metal intercalated fullerides. The additional term due to electron–electron contribution was required in understanding the resistivity behavior, as extensive attempts to fit the data with residual resistivity and phonon resistivity were unsuccessful. The magnitude of the resistivity is high for a metallic system, indicating a small density of carriers participating in the electrical conduction.

The zero temperature-limited resistivity is also a large fraction of the total resistivity at room temperature, which suggests that a large amount of impurity scattering is present. The large residual scattering is also susceptible to the phonon drag, and as a consequence, it decreases even in the single crystals. This presence of strong elastic scattering of electrons due to disorder may play a role in reducing the temperature dependence due to scattering by phonons below the T^5 behavior seen in good metals with small elastic scattering, or the power temperature behavior may arise from electron–electron scattering in Fermi liquid. We have thus demonstrated that apart from electron–phonon, electron–electron scattering is also important. Henceforth, using the resistivity probe, we have carefully examined the normal state resistivity in AMIF and found that power temperature dependence is essentially of the same feature as those revealed in electron doped cuprate and in alkali metal-doped barium bismuthate superconductors.

In conclusion, the electron pairing in fulleride superconductors and a consistent interpretation of the properties *viz.* transition temperature, carbon isotope effect, energy gap parameter, pressure and volume effect on T_c, thermodynamical parameters describing the superconducting state, and normal state electrical resistivity reveal the fact that both the Coulomb and electron–phonon (inter- and intra-molecular) are important interactions in examining the unusual physical properties in alkali metal intercalated fulleride superconductors. The results are of interest and provide a test of the possibility of the cooperative mechanism in other doped fullerides.

Competing interests
The authors declare that they have no competing interests.

Authors' contributions
DV suggested and formulated the problem for investigation. RJ and NS are essentially involved in the computation of all physical parameters. All authors have equally participated in drawing conclusions, writing results and complete the paper. All authors read and approved the final manuscript.

Authors' information
DV is professor in the School of Physics, Devi Ahilya University, Indore, India. RJ is pursuing research in the School of Physics, Devi Ahilya University, Indore, India. NS is an assistant professor in the Department of Physics, Ranchi College, Ranchi University Ranchi.

Author details
[1]Materials Science Laboratory, School of Physics, Vigyan Bhawan, Devi Ahilya University, Khandwa Road Campus, Indore 452001, India. [2]Department of Physics, Ranchi College, Ranchi University Ranchi, Jharkhand 834008, India.

Received: 20 July 2012 Accepted: 4 October 2012
Published: 24 October 2012

References

1. Hebard, AF, Rosseinsky, MJ, Haddon, RC, Murphy, DW, Glarum, SH, Palstra, TTM, Ramirez, AP, Kortan, AR: Superconductivity at 18 K in potassium-doped C_{60}. Nature **350**, 600 (1991)
2. Tanigaki, K, Ebbessen, TW, Saito, S, Mizuki, J, Tsai, JS, Kubo, Y, Kurushima, S: Superconductivity at 33 K in $Cs_xRb_yC_{60}$. Nature **352**, 222 (1991)
3. Holczer, K, Klein, O, Huang, SM, Kaner, RB, Fu, KJ, Whetten, RL, Diederich, FN: Alkali-fulleride superconductors: synthesis, composition, and diamagnetic shielding. Science **252**, 600 (1991)
4. Forro, L, Mihaly, L: Electronic properties of doped fullerenes. Rep Prog. Phys. **64**, 649 (2001)
5. Gunnarson, O: Superconductivity in fullerides. Rev. Mod. Phys. **69**, 575 (1997)
6. Pintschovius, L: Neutron studies of vibrations in fullerenes. Rep. Prog. Phys. **59**, 473 (1996)
7. Prassides, K, Tomkinson, J, Christides, C, Rosseinsky, MJ, Murphy, DW, Haddon, RC: Vibrational spectroscopy of superconducting K_3C_{60} by inelastic neutron scattering. Nature **354**, 462 (1991)
8. Mitch, MG, Chase, SJ, Lannian, JS: Raman scattering and electron–phonon coupling in Rb_xC_{60}. Phys. Rev. Lett. **68**, 883 (1992)
9. Belosludov, VR, Shpakov, VP: Lattice-dynamics study of K_3C_{60}. Mod. Phys. Lett. **6**, 1209 (1991)
10. Ebbesen, TW, Tsai, JS, Tanigaki, K, Hiura, H, Shimakawa, Y, Kubo, Y, Hirosawa, T, Mizuki, J: Dopant isotope effect on superconductivity in Rb_3C_{60}. Physica C **203**, 163 (1992)
11. Fuhrer, S, Cherrey, K, Zettl, A, Cohen, ML: Carbon isotope effect in single-crystal Rb_3C_{60}. Phys. Rev. Lett. **83**, 404 (1999)
12. Burk, B, Crespi, VH, Zettl, A, Cohen, ML: Rubidium isotope effect in superconducting Rb_3C_{60}. Phys. Rev. Lett. **72**, 3706 (1994)
13. Stritzker, B, Buckel, W: Superconductivity in the palladium-hydrogen and the palladium-deuterium systems. Z Phys B **257**, 1 (1972)
14. Klein, BM, Cohen, RE: Anharmonicity and the inverse isotope effect in the palladium-hydrogen system. Phys. Rev. B **45**, 12405 (1992)
15. Uemura, YJ, Keren, A, Le, LP, Luke, GM, Sternlieb, BJ, Wu, WD, Brewer, JH, Whetten, RL, Huang, SM, Lin, S, Kaner, RB, Diederich, F, Donovan, S, Gruner, G, Holczer, K: Magnetic-field penetration depth in K_3C_{60} measured by muon spin relaxation. Nature **352**, 605 (1991)
16. Zhang, Z, Chen, CC, Kelty, SP, Dai, H, Lieber, CM: The superconducting energy gap of Rb_3C_{60}. Nature **353**, 333 (1991)
17. Degiorgi, L, Gruner, G, Wachter, P, Huang, SM, Wiley, J, Whetten, RL, Kaner, RB, Holczer, K, Diederich, F: Electrodynamic response of Rb_3C_{60}. Phys. Rev. B **46**, 11250 (1992)
18. Rotter, LD, Schlesinger, Z, McCauley Jr, JP, Coustel, N, Fischer, JE, Smith III, AB: Infrared reflectivity measurements of a superconducting energy scale in Rb_3C_{60}. Nature **355**, 532 (1992)
19. Kiefl, RF, MacFarlane, WA, Chow, KH, Dunsiger, S, Duty, TF, Johnston, TMS, Schneider, JW, Sonier, J, Brad, L, Strongin, RM, Fischer, JE, Smith III, AB: Coherence peak and superconducting energy gap in Rb_3C_{60} observed by muon spin relaxation. Phys. Rev. Lett. **70**, 3987 (1993)
20. Tyck, OR, Dabbagh, G, Rosseinsky, MJ, Murphy, DW, Ramirez, AP, Fleming, RM: Electronic properties of normal and superconducting alkali fullerides probed by ^{13}C nuclear magnetic resonance. Phys. Rev. Lett. **68**, 1912 (1992)
21. Holczer, K, Klein, O, Allou, H, Yoshinari, Y, Hippert, F, Huang, SM, Kaner, RB, Whetten, RL: Non-Korringa ^{13}C nuclear relaxation in the normal state of the K_3C_{60} superconductor. Europhys. Lett. **23**, 63 (1993)
22. Degiorgi, L, Wachter, P, Gruner, G, Huang, SM, Wiley, J, Kaner, RB: Optical response of the superconducting state of K_3C_{60} and Rb_3C_{60}. Phys. Rev. Lett. **69**, 2987 (1992)
23. Koller, D, Martin, MC, Mihaly, L, Mihaly, G, Oszlanyi, G, Baumgartner, G, Forro, L: Energy gap in superconducting fullerides: optical and tunneling studies. Phys. Rev. Lett. **77**, 4082 (1996)
24. Gu, C, Veal, BW, Liu, R, Paulikas, AP, Kostic, P, Ding, H, Gofron, K, Campuzano, JC: Electronic structure and superconducting energy gap in Rb_3C_{60} single crystals studied by photoemission spectroscopy. Phys. Rev. B **50**, 16566–16569 (1994)
25. Zhang, Z, Chen, CC, Lieber, CM: Tunneling spectroscopy of M_3C_{60} superconductors: the energy gap, strong coupling, and superconductivity. Science **254**, 1619 (1991)
26. Zhang, FC, Ogata, M, Rice, TM: Attractive interaction and superconductivity for K_3C_{60}. Phys. Rev. Lett. **67**, 3452 (1991)
27. Varma, CM, Zaanen, J, Raghavachari, K: Superconductivity in the fullerenes. Science **254**, 989 (1991)
28. Schluter, M, Lanoo, M, Needels, M, Baratt, GA, Tomanek, D: Electron–phonon coupling and superconductivity in alkali-intercalated C_{60} solid. Phys. Rev. Lett. **68**, 526 (1992)
29. Kresin, VZ, Wolf, SA: Induced superconducting state and two-gap structure: application to cuprate superconductors and conventional multilayers. Phys. Rev. B **46**, 6458–6471 (1992)
30. Kresin, VZ: Coupling strength in superconducting fullerenes. Phys. Rev. B **46**, 1833 (1992)
31. Zhang, ML, Guo, HY: Electron–phonon interaction of the C_{60} intra-molecule mode in A_3C_{60}. Physics Letters A **191**, 189 (1994)
32. Ivanov, V, Maruyama, Y: Disorder and phonon windows for superconductivity in doped fullerides. Physica C **247**, 147 (1995)
33. Alexandrov, AS, Kabanov, VV: Theory of superconducting T_c of doped fullerenes. Phys. Rev. B **54**, 3655 (1996)
34. Sparn, G, Thompson, JD, Whetten, RL, Huang, SM, Kaner, RB, Diederich, F, Gruner, G, Holczer, K: Pressure and field dependence of superconductivity in Rb_3C_{60}. Phys Rev Lett **68**, 1228 (1992)
35. Sparn, G, Thompson, JD, Huang, SM, Kaner, RB, Diederich, F, Whetten, RL, Gruner, G, Holczer, K: Pressure dependence of superconductivity in single-phase K_3C_{60}. Science **252**, 1829 (1991)
36. Diederich, J, Gangopadhyay, AK, Schilling, JS: Pressure dependence of the electronic density of states and T_c in superconducting Rb_3C_{60}. Phys. Rev. B **54**, R 9662 (1996)
37. Chaban, IA: Pressure effect in high-temperature superconductors and fullerides. J. Supercond. Incorp. Nov. Mag. **15**, 179 (2002)
38. Satapthy, S, Antropov, VP, Anderson, OK, Jepsen, O, Gunnarson, O, Liechtension, IA: Conduction-band structure of alkali-metal-doped C_{60}. Phys. Rev. B **46**, 1773 (1992)
39. Kochanski, GP, Hebard, AF, Haddon, RC, Fiory, AT: Electrical resistivity and stoichiometry of K_xC_{60} films. Science **255**, 184 (1992)
40. Palstra, TTM, Haddon, RC, Hebard, AF, Zaaren, J: Electronic transport properties of K_3C_{60} films. Phys. Rev. Lett. **684**, 1054 (1992)

41. Xiang, XD, Hou, JG, Briceno, G, Vareka, WA, Mostovoy, R, Zettl, A, Crespi, VH, Cohen, ML: Synthesis and electronic transport of single crystal K_3C_{60}. Science **256**, 1190 (1992)
42. Hou, JG, Crespi, VH, Xiang, XD, Vareka, WA, Briceno, G, Zettl, A, Cohen, ML: Determination of superconducting and normal state parameters of single crystal K_3C_{60}. Sol. State Comm. **86**, 643 (1993)
43. Morelli, DT: Thermoelectric power of superconducting fullerenes. Phys. Rev. B **49**, 655 (1994)
44. Cohen, ML: Theory of normal and superconducting properties of fullerene-based solids. Mater. Science Engg. B **19**, 111 (1993)
45. Gelfand, MP, Lu, JP: Orientational disorder and normal-state electronic-transport properties of A_3C_{60}. Phys. Rev. B **46**, 4367 (1992)
46. Crespi, VH, Hou, JG, Xiang, XD, Cohen, ML, Zettl, A: Electron-scattering mechanisms in single-crystal K_3C_{60}. Phys. Rev. B **46**, 12064 (1992)
47. Hou, JG, Lu, L, Crespi, VH, Xiang, XD, Zettl, A, Cohen, ML: Resistivity saturation in alkali-doped C_{60}. Sol. State Comm. **93**, 973 (1995)
48. Martins, JL, Troullier, N: Structural and electronic properties of K_nC_{60}. Phys. Rev. B **46**, 1766 (1992)
49. Erwin, SC, Pickett, WE: Theoretical normal-state transport properties of K_3C_{60}. Phys. Rev. B **46**, 14257 (1992)
50. Erwin, SC, Pickett, WE: Theoretical Fermi-surface properties and superconducting parameters for K_3C_{60}. Science **254**, 842 (1991)
51. Maraduddin, AA, Montroll, EW, Weiss, GH: Theory of Lattice Dynamics in the Harmonic Approximation. Solid State Physics Supplement, vol. 3rd edn. Academic, NewYork (1963)
52. Khalatnikov, IM, Abrikosov, AA: The modern theory of superconductivity. Usp. Fiz. Nauk **65**, 551 (1958) English translation in Adv Phys **8**, 45 (1959)
53. Bogoliubov, NN, Tolmachev, VV, Shirkov, DD: A New Method in the Theory of Superconductivity. Consultants Bureau, NewYork (1959)
54. Eliashberg, GM: Interactions between electrons and lattice vibrations in a superconductor. Sov. Phys JETP **11**, 696 (1960)
55. Eliashberg, GM: Temperature greens function for electrons in a superconductor. Sov. Phys JETP **12**, 1000 (1961)
56. Morel, P, Anderson, PW: Calculation of the superconducting state parameters with retarded electron–phonon interaction. Phys. Rev. **125**, 1263 (1962)
57. McMillan, WL: Transition temperature of strong-coupled superconductors. Phys. Rev. **167**, 331 (1968)
58. Novikov, DL, Gubanov, VA, Freeman, AJ: Electronic structure, electron–phonon interaction and superconductivity in K_3C_{60}, Rb_3C_{60} and Cs_3C_{60}. Physica C **191**, 399 (1992)
59. Huffman, DR: Solid C_{60}. Phys. Today **44**, 22 (1991)
60. Hebard, F: Superconductivity in doped fullerenes. Phys. Today **45**, 26 (1992)
61. Hebard, AF, Haddon, RC, Fleming, RM, Kortan, AR: Deposition and characterization of fullerene films. Appl. Phys. Lett. **59**, 2109 (1991)
62. Kresin, VZ: On the critical temperature for any strength of the electron–phonon coupling. Phys. Lett. A **122**, 434 (1992)
63. Cappelluti, E, Grimaldi, C, Pietronero, L, Strassler, S, Ummarino, GA: Superconductivity of Rb_3C_{60}: breakdown of the Migdal-Eliashberg theory. Eur. Phys. J. B **21**, 383 (2001)
64. Cappelluti, E, Grimaldi, C, Pietronero, L, Strassler, S: Nonadiabatic channels in the superconducting pairing of fullerides. Phys. Rev. Lett. **85**, 4771 (2000)
65. Alexandrov, AA: Breakdown of the Migdal-Eliashberg theory in the strong-coupling adiabatic regime. Eur. Phys. Lett. **56**, 92 (2001)
66. Johnson, RD, Bethune, DS, Yannoni, CS: Fullerene structure and dynamics: a magnetic resonance potpourri. Acc. Chem. Res. **25**, 169 (1992)
67. Ramirez, AP, Kortan, AR, Rosseinsky, MJ, Duclos, SJ, Mujsce, AM, Haddon, RC, Murphy, DW, Makhija, AV, Zahurak, SM, Lyons, KB: Isotope effect in superconducting Rb_3C_{60}. Phys. Rev. Lett. **68**, 1058 (1992)
68. Holczer, K, Whetten, RL: Superconducting and normal state properties of the A_3C_{60} compounds. Carbon **30**, 1261 (1992)
69. Sololov, AI, Kufaev, YA, Sonin, EB: Penetration depth and Ginzburg number in Rb_3C_{60}. Physica C **212**, 19 (1993)
70. Degiorgi, L, Nicol, EJ, Klein, O, Gruner, G, Watcher, P, Huang, SM, Wiley, J, Kaner, RB: Optical properties of the alkali-metal-doped superconducting fullerenes: K_3C_{60} and Rb_3C_{60}. Phys. Rev. B **49**, 7012 (1994)
71. Foner, S, McNiff Jr, EJ, Heiman, D, Huang, SM, Kaner, RB: Measurements of the upper critical field of K_3C_{60} and Rb_3C_{60} powders to 60 T. Phys. Rev. B **46**, 14936 (1992)
72. Olsen, JL, Bucher, E, Levy, M, Muller, J, Corenzwit, E, Geballe, T: Superconductivity under pressure. Rev. Mod. Phys. **36**, 168 (1964)
73. Crespi, VH, Cohen, ML: Near constancy of the pressure dependence of T_c across families of organic and fullerene superconductors. Phys. Rev. B **53**, 56 (1996)
74. Crespi, VH, Cohen, ML: Scattering mechanisms in Rb-doped single-crystal C_{60}. Phys. Rev. B **52**, 3619 (1995)
75. Carbotte, JP: Properties of boson-exchange superconductors. Rev. Mod. Phys. **62**, 1027 (1990)
76. Deutscher, G, Entin-Wohlman, O, Fishman, S, Shapira, Y: Percolation description of granular superconductors. Phys. Rev. B **21**, 5041 (1980)
77. Grimvall, G: The electron–phonon interaction in metals. North Holland Publishing Company, Netherlands (1981)
78. Varshney, D, Choudhary, KK, Singh, RK: Interpretation of temperature-dependent resistivity of electron doped cuprates. Supercond. Sci. Technol. **15**, 1119 (2002)
79. Varshney, D, Shah, S, Singh, RK: Superconductivity and normal state resistivity of $Ba_{0.6}K_{0.4}$ BiO_3: an optical phonon approach. Superlattice Microst **24**, 409 (1998)
80. Thompson, AH: Electron–electron scattering in TiS_2. Phys. Rev. Lett. **35**, 1786 (1975)
81. Chida, T, Suzuki, S, Nakao, K: Theoretical study on anomalous behaviors in photoemission spectra of alkali-metal-doped C_{60}. J. Phys. Soc. Jpn. **71**, 525 (2002)
82. Knufper, M, Fink, J: Mott-Hubbard-like behavior of the energy gap of A_4C_{60} (A = Na, K, Rb, Cs) and $Na_{10}C_{60}$. Phys. Rev. Lett. **79**, 2714 (1997)
83. Varshney, D: Effect of pressure on transition temperature of Rb_3C_{60} fullerides. High Pressure Res. **26**, 203 (2006)
84. Varshney, D, Dubey, A, Choudhary, KK, Singh, RK: Superconductivity and electrical resistivity in alkali doped fullerides: phonon mechanism. Bull. Mater. Sci. **28**, 155 (2005)
85. Varshney, D, Kaurav, N, Dubey, A, Singh, RK: Low temperature heat capacity and Coulomb correlations of K_3C_{60}. Synth. Met. **155**, 380 (2005)
86. Varshney, D, Kaurav, N, Choudhary, KK: Electrical transport in the normal state of K_3C_{60} fullerides: polaron conduction. Supercond. Sci. Technol. **18**, 1259 (2005)
87. Varshney, D, Dube, A: Interpretation of temperature dependent resistivity of K_3C_{60} fullerides superconductors: electron–phonon mechanism. Supercond. Sci. Technol. **17**, 1231 (2004)
88. Varshney, D: Pairing mechanism and superconductivity of Rb_3C_{60} alkali fullerides. J. Supercond. Inc. Nov. Mag. **13**, 171 (2000)
89. Varshney, D, Varshney, M, Singh, RK, Mishra, R: Superconductivity in alkali metal doped fullerenes K_3C_{60}: a phonon mechanism. J. Phys. Chem. Solids **60**, 579 (1999)
90. Varshney, D, Varshney, M, Singh, RK, Mishra, R: Analysis of normal state resistivity of single crystal K_3C_{60} superconductors. Supercond. Sci. Technol. **11**, 1300 (1998)
91. Varshney, D, Singh, RK: Electron–electron and electron–phonon interactions in alkali doped fullerenes: implications for resistivity. Physica C **282**, 1919 (1997)

doi:10.1186/2251-7235-6-25
Cite this article as: Varshney *et al.*: **Phonon-induced superconductivity and physical properties in intercalated fullerides Rb_3C_{60}.** *Journal of Theoretical and Applied Physics* 2012 **6**:25.